이학석사 학위논문

Molecular Design for the Tuning of Membrane Properties of Self-Assembled Nanostructures of Block Copolymers and their Applications

블록 공중합체의 자기조립 구조체 형성을 위한 막특성 조절 가능한 합성 디자인과 응용 연구

2023 년 2 월

서울대학교 대학원

화학부 고분자화학 전공

Wang Valene Man Lin

Molecular Design for the Tuning of Membrane Properties of Self-Assembled Nanostructures of Block Copolymers and their Applications

지도 교수 김 경 택

이 논문을 이학석사 학위논문으로 제출함

2023 년 2 월

서울대학교 대학원

화학부 고분자화학 전공

Wang Valene Man Lin

Wang Valene Man Lin 의 이학석사 학위논문을 인준함

2023 년 2 월

위 원 장 손 병 혁 (인)

부위원장 김 경 택 (인)

위 원 이 홍 근 (인)

ABSTRACT

The modulation of shape and morphologies of self-assembled nanostructures formed by the solution self-assembly of block copolymers continues to be of significance due to their potential applications including drug delivery, nanoreactors and nanotemplates. Furthermore, the design of the block copolymers (BCPs) by integrating stimuli-responsive and supramolecular moieties which is rendered possible by the utilization of monodisperse blocks, provides contactless and less intensive synthetic work to obtain desired shapes and morphologies.

In Chapter 1, amphiphilic block copolymers (BCPs) composed of hydrophilic polyethylene glycol (PEG) blocks and discrete oligo(phenyllactic acid) (OPLA) blocks with hydrazone-based photoswitches at specific positions, naming (1) in the middle of the hydrophobic OPLA chains, and (2) at the junction of the hydrophilic and hydrophobic blocks. The photoswitch undergoes *E*-*Z* isomerization, resulting in the conformational change of the OPLA block. Notably, the polymer vesicles exhibited reversible shape transformation upon irradiation with UV or visible light due to the configurational switching of the photoswitch.

In Chapter 2, we reported the synthesis of block copolymers (BCPs) composed of tri-arm linear, conventional linear and crown ether end-functionalized hydrophilic polyethylene glycol (PEG) blocks, and hydrophobic polystyrene (PS) blocks. The addition of lithium ions induces salting-out effect at different extents for different BCPs based on the architecture and end-group functionalized hydrophilic segments. The interplay of salting-out effect and host-guest recognition between 12-crown-4 ether and lithium cation also contribute significantly to the morphological transformation from pristine polymersomes to polymer cubosomes.

Keywords : hydrazone photoswitch, oligo(phenyl lactic acid), polyethylene glycol, crown ether, block copolymer, solution self-assembly, polymer vesicles, polymer cubosomes

Student Number : 2020-27163

Table of Contents

List of Figures, Schemes, and Tables

Figures

Schemes

Tables

Chapter 1. On-demand shape transformation of polymer vesicles via site-specific isomerization of hydrazone photoswitches in monodisperse hydrophobic oligomers

1.1 Abstract

The shape control of nanostructures formed by the solution self-assembly of block copolymers is of significance for drug delivery. In particular, site-specific perturbation resulting in the conformational change of the hydrophobic block has attracted considerable attention because of the possibility of creating polymer vesicles capable of releasing cargo molecules on demand by responding to specific stimuli. Herein, we report the synthesis of amphiphilic block copolymers based on the monodisperse molecular-weight oligo(phenyllactic acid) (OPLA) having hydrazone photoswitches at specific locations. Upon light irradiation, the photoswitch undergoes *E*-*Z* isomerization, resulting in the conformational change of the OPLA block. Polymer vesicles composed of these block copolymers exhibited reversible shape transformation upon irradiation with UV or visible light due to the *E*-*Z* isomerization of the photoswitch. Furthermore, the location and the number of hydrazone photoswitches in the monodisperse OPLA block are the decisive factors for the reversible shape transformation of the polymer vesicles from an isotropic to an anisotropic morphology.

1.2 INTRODUCTION

Stimuli-responsive polymer vesicles (polymersomes) have been extensively investigated as intelligent vehicles for on-demand drug delivery in response to chemical, physical, and biological stimuli.[1–6] When the compartmentalizing membranes of polymersomes are exposed to external stimuli, the polymersomes release the guest molecules encapsulated in their cavity via molecular transport through the bilayer membrane consisting of self-assembled block copolymers (BCPs). Generally, the transmembrane transport of guest molecules require pore generation in the polymersome membranes, which occurs through the solubility switching of the BCP building blocks or pore generators embedded in the membrane; this leads to the disassembly or perforation of the membranes under specific external stimuli such as pH, temperature, biomolecules and light.[7–10]

Zhang et al. demonstrated the transition of the packing state of the vesicular membrane from tight packing to loose stacking, generate defects which increases mechanical instability and cause the formation of pores on the membrane for fusion and fission to occur.[11] Li et al. found that photoinduced assembly and disassembly was due to the change in dipole moment which induces a shift in the hydrophilic/ hydrophobic balance which in turn determines the solubility difference.[12] Li and co-workers designed a compartmentalizing membrane that facilitates mass transport via rupture, based on the concept of liquid crystalline (LC)-isotropic phase transition of azobenzene mesogens which drives spontaneous curvature and curling instability.[13] However, pore generation based on these mechanisms can cause permanent perforation of the membranes or complete disassembly of the polymersomes.[13–15] Therefore, the development of polymersomes that can reversibly release or retain the encapsulated cargo molecules under external stimuli has attracted recent interest.[16]

In this regard, the photo-triggered release of guests from polymersomes composed of photo-responsive BCPs has been extensively investigated because these polymersomes enable reversible mass transport through the bilayers without the permanent disruption of the vesicular membrane.[17] The permeability of these polymersomes can be changed by inducing the conformational change of the membrane-forming BCPs in response to a certain light wavelength.[18] To achieve the light-triggered conformational change of polymers, photoisomerizable azobenzene groups are routinely introduced as photoswitches in BCPs. Recently, Thayumanavan et al. took an alternative approach known as interface-induced dynamic facilitation, which promotes propagation across a glassy polymeric membrane via the configurational switching of a single azobenzene unit.[19]

Most photo-responsive BCPs are synthesized by controlled polymerization methods involving the introduction of photo-responsive units as pendent groups [11,12,20–32] on the polymer backbone or at the junction interfacing the constituting polymer blocks.[19,33–36] However, studying the effect of the location of the photoswitch in polymeric systems on their conformational change using traditional polymerization techniques is challenging. We envisioned that the synthesis of discrete hydrophobic blocks using a convergent approach would allow a more sophisticated control over the position of the photoswitch incorporated in the hydrophobic core and thus help understand the relationship between the structure and actuation of the self-assembled BCPs.

Herein, we report the synthesis of BCPs composed of hydrophilic polyethylene glycol (PEG) blocks and discrete oligo(phenyllactic acid) (OPLA) blocks with hydrazone-based photoswitches at specific positions. To determine the effect of the light-induced configurational switching of the photoswitches, they were embedded in two different positions within the BCP chains: (1) in the middle of the

hydrophobic OPLA chains, and (2) at the junction of the hydrophilic and hydrophobic blocks. Moreover, to investigate the effect of the number of photoswitches in the BCP backbone on the extent of the shape transformations of the self-assembled nanostructures, a BCP containing multiple photoswitches was synthesized. The shape transformation of the self-assembled nanostructures of these BCPs were triggered by the *E*/*Z* isomerization of the hydrazone-based photoswitches upon irradiation with a light source (λ = 405 nm or 365 nm), which changed the conformation of the discrete OPLA blocks. The polymersomes exhibited reversible shape transformation via the *E*/*Z* isomerization of the hydrazone photoswitch embedded in the discrete hydrophobic block. The effect of the conformational change of the hydrophobic block on the shape transformation of the BCP-based polymersomes was even more pronounced when the number of hydrazone switches was increased. The present study highlights the importance of the perfect control of the position of a versatile hydrazone photoswitch in BCPs for the configurational change at the nanoscale to be translated to microscopic actuation of the BCP membrane, i.e., shape transformation. The elucidation of the on-demand actuation of our system can open new avenues for the tailoring of polymeric morphologies for versatile applications.

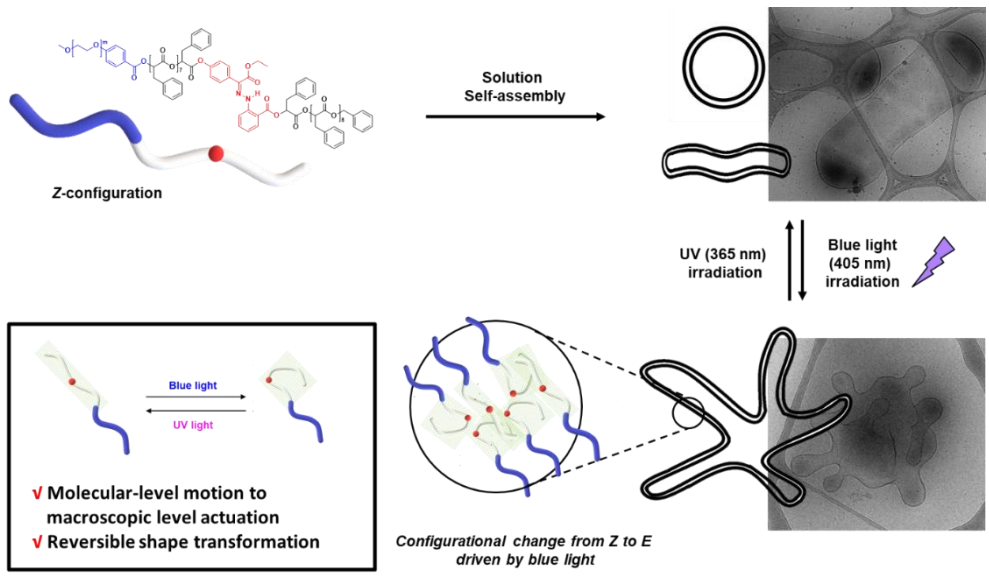

Fig. 1-1 Schematic representation of the reversible shape transformation of self-assembled structures of PEG-*b*-[OPLA] containing hydrazone-based photoswitches via configurational switching of the system.

1.3 RESULTS AND DISCUSSION

1) Effect of the position of hydrazone photoswitches in the BCP backbone

Hydrazone-based photoswitches contain the C=N-NH functional group, renders the system virtually bistable (thermal relaxation ($\tau_{1/2}$) up to 5,300 years).[37,38] This characteristic of hydrazone photoswitches can be ideal for permanently locking the actuation of dynamic molecules for the on-demand sustained release of guest molecules.[39] The hydrazone-based photoswitch (H1) was synthesized using a previously reported procedure (Scheme 1-3 and Fig. 1-9).[40]

To prepare discrete hydrophobic blocks, OPLAs of different molecular weights were synthesized by iterative convergent methods (Scheme 1-1 and 1-4).[41,42] The orthogonally protected dimer of phenyllactic acid, TBDMS-$OPLA_2$-Bz, was deprotected to prepare HO-$OPLA_2$-Bz and TBDMS-$OPLA_2$-COOH by desilylation with BF_3 and hydrogenation, respectively. The deprotected $OPLA_2$ compounds were coupled by esterification using N-(3-dimethylaminopropyl)-N'-ethylcarbodiimide (EDC) as a coupling agent. The resulting TBDMS-$OPLA_4$-Bz was used for further convergence to obtain $OPLA_8$ and $OPLA_{16}$ (Scheme 1-1 and 1-5). The discrete OPLAs were purified by column chromatography, and their purity was determined by NMR spectroscopy and matrix-assisted laser desorption/ionization time-of-flight (MALDI-TOF) mass spectrometry (Fig. 1-11, 1-12, 1-13 and 1-14).

Using the discrete OPLAs as building blocks, we synthesized discrete hydrophobic blocks by introducing a photoswitch, H1, at the desired position in the

polymer backbone. We first synthesized discrete $OPLA_{17}$ by coupling two $OPLA_8$ units using H1 as a linker. To connect the OPLAs via the H1 linker, a single unit of phenyllactic acid was used as a spacer between H1 and the OPLAs. To introduce H1 in the mid-position of the OPLA block, OH-$OPLA_8$ was reacted with H1-PLA_1-COOH using EDC as a coupling agent. After acetal deprotection with PPTS, the resulting OH-H1-$OPLA_9$ was esterified with $OPLA_8$-COOH to obtain a monodisperse hydrophobic block $OPLA_8$-H1-$OPLA_9$ with the photoswitch in the middle of the oligomer backbone (Scheme 1-2, 1-7, Fig. 1-15 and 1-16). To introduce H1 at the junction of the hydrophilic and OPLA blocks, H1-$OPLA_{17}$ was synthesized by the esterification of H1-PLA_1-COOH and OH-$OPLA_{16}$ (Scheme 1-8). The synthesized hydrophobic block was characterized by ^{1}H NMR spectroscopy and MALDI-TOF mass spectrometry (Fig. 1-2A, 1-2B, 1-19A and 1-19B).

The synthesis of BCPs composed of a discrete hydrophobic block H1 at different positions and a hydrophilic PEG block of different molecular weights (M_n = 550 and 1000) was confirmed by ^{1}H NMR spectroscopy and MALDI-TOF spectrometry (Fig. 1-2C, 1-2D, 1-17, 1-18, 1-19C, 1-19D and 1-20); the results are summarized in Table 1-1.

The ^{1}H NMR spectroscopic analysis of the as-prepared H1 in DMSO revealed that H1 exclusively adopts the *Z*-configuration (>99%) at room temperature (Fig. 1-10). Irradiation with 405 nm light yielded a photostationary state (PSS) consisting of 90% *E*-H1, while irradiation of the resulting solution with UV light (365 nm) yielded a mixture consisting of 70% *Z*-H1 at the PSS (Fig. 1-10A and 1-10B). In addition, UV-Vis spectroscopy was conducted for photoisomerization studies (Fig. 1-10C). The switching cycles of H1 in DMSO under alternating light irradiation were confirmed from the absorbance change at 373 nm (Fig. 1-10D). The photoisomerization of the prepared **BCP1** (PEG550-*b*-[$OPLA_8$-H1-$OPLA_9$])

was studied and monitored by ^{1}H NMR spectroscopy in $CDCl_3$ (Fig. 1-3, 1-21 and 1-22). The irradiation of BCP containing *Z*-**BCP1** (>99%) with blue light (λ = 405 nm) yielded a PSS consisting of 85% *E*-**BCP1**, while the irradiation of the resulting solution with UV light (365 nm) yielded a mixture containing 91% of the *Z* isomer at the PSS (Fig. 1-3B and 1-3C). The degree of conversion between *E*- and *Z*-isomers of H1 embedded in BCP is comparable to that of an individual H1 molecule, which proves the functionality of H1 in the BCP. The isomerization of H1 in the self-assembled structures of **BCP1** was studied by UV-Vis absorption spectroscopy over time (Fig. 1-23). Although the isomerization rate of H1 embedded in the BCP membrane was decreased, the photoisomerization was not compromised which resulted in shape transformation of the polymersomes.

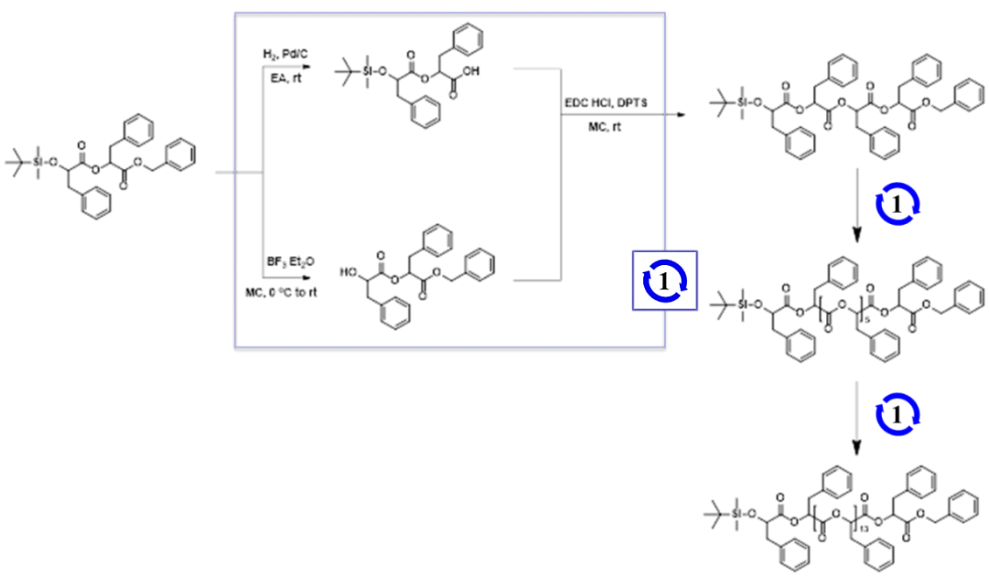

Scheme 1-1 Synthesis of discrete oligo(phenyl lactic acid)s (OPLAs).

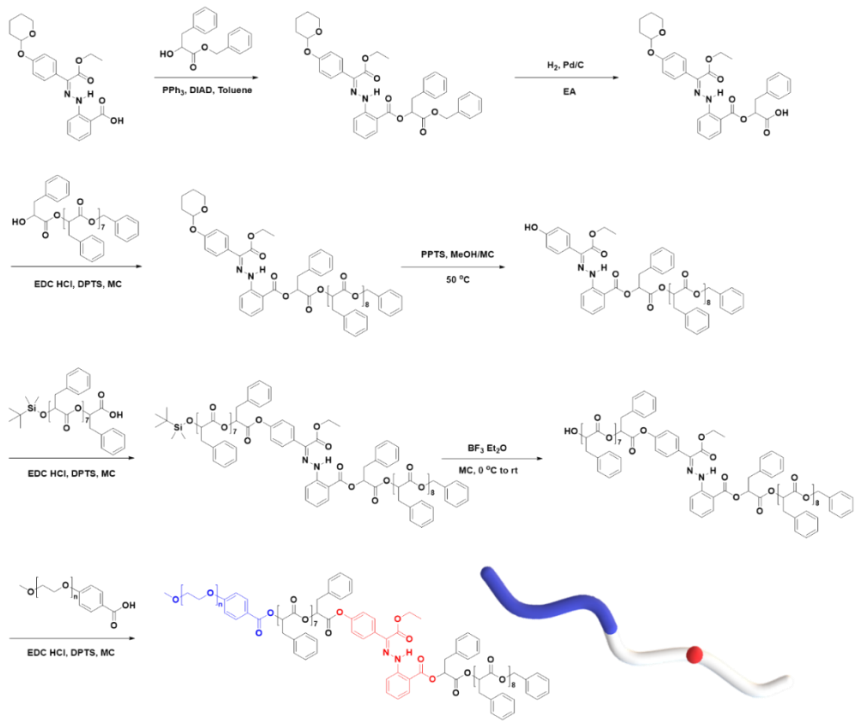

Scheme 1-2 Synthesis of BCP having hydrazone-based photo-switches (PEG-*b*-[OPLA$_8$-H1-OPLA$_9$]).

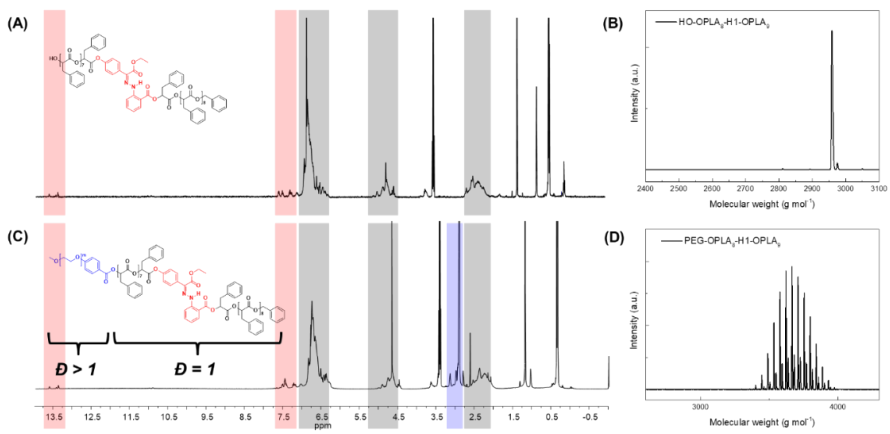

Fig. 1-2 (A and C) ^{1}H NMR spectra in $CDCl_3$ and (B and D) MALDI-TOF spectra of monodisperse hydrophobic block (HO-OPLA$_8$-H1-OPLA$_9$) and amphiphilic block copolymer (PEG550-*b*-[OPLA$_8$-H1-OPLA$_9$]), respectively.

Table 1-1 Characteristics of amphiphilic block copolymers containing photoswitch.

Sample	Name	Position of H1	M_n (g/mol)[a] of hydrophobic block	M_n (g/mol)[a] of hydrophilic block	$Đ$[a] of BCPs	f_{PEG} (%)[b]
1	PEG550-*b*-[$OPLA_8$-H1-$OPLA_9$]	Center	2958	550	1.02	15.7
2	PEG550-*b*-[H1-$OPLA_{17}$]	Junction	2958	550	1.02	15.7
3	PEG1000-*b*-[$OPLA_8$-H1-$OPLA_9$]	Center	2958	1000	1.02	25.2
4	PEG1000-*b*-[H1-$OPLA_{17}$]	Junction	2958	1000	1.02	25.2
5	PEG1000-*b*-[$OPLA_4$-H1-$OPLA_8$-H1-$OPLA_4$]	Center	3100	1000	1.02	24.4

[a]Number average molecular weight (M_n) and molecular weight distribution ($Đ$) determined by GPC using polystyrene (PS) standards. Elution was performed with THF at a flow rate of 1 mL min^{-1} at 30 °C. [b]Molecular weight fraction of the PEG domain relative to the amphiphilic block copolymer.

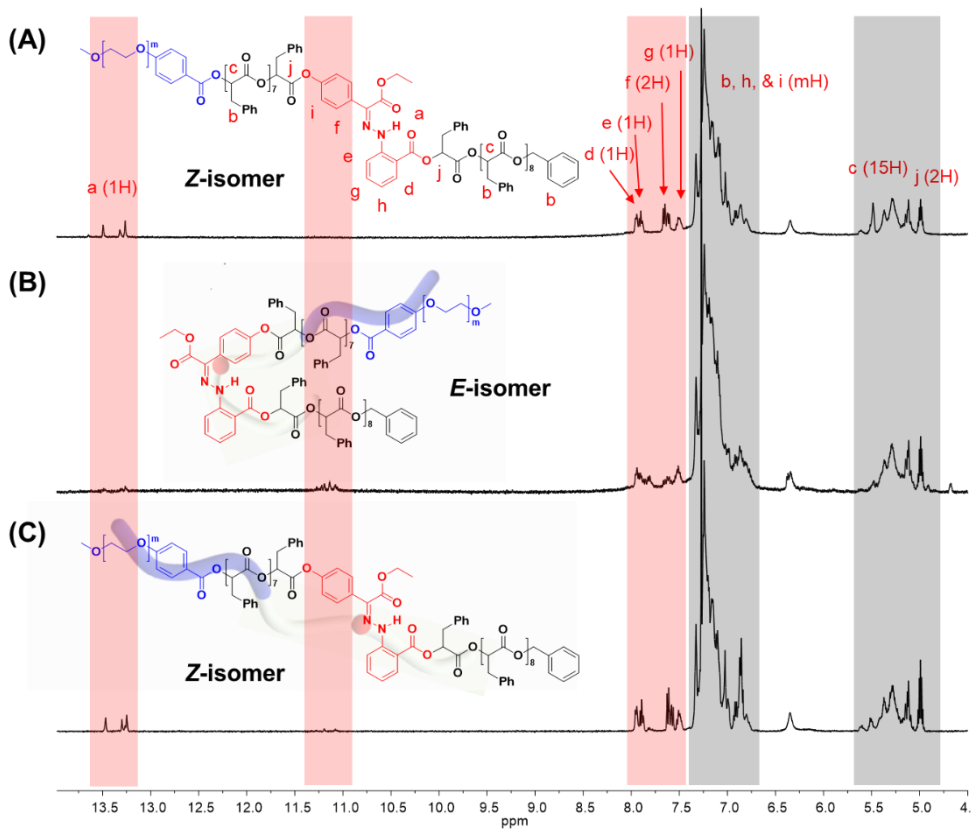

Fig. 1-3 ^{1}H NMR spectra of amphiphilic block copolymer containing hydrazone-based photoswitches (A) before and (B) after irradiation with blue light (405 nm), followed by (C) photoirradiation with UV light (365 nm).

Shape transformations of BCP1 and BCP2 containing PEG550 as hydrophilic blocks under different light sources.

Two BCPs composed of the hydrophilic PEG block (M_n = 550 Da, $Đ$ = 1.02) and hydrophobic blocks ($Đ$ = 1) with H1 placed at different positions, were dissolved in acetone used as a common solvent at a concentration of 5 mg mL^{-1}. Subsequently, to prepare the nanostructures, distilled water as a selective solvent was slowly added at a rate of 0.5 mL h^{-1} using a syringe pump. The resulting dispersion was dialyzed against water for 24 h to remove organic solvents. Transmission electron microscopy (TEM) analysis revealed that **BCP1** (PEG550-*b*-[$OPLA_8$-H1-$OPLA_9$]) and **BCP2** (PEG550-*b*-[H1-$OPLA_{17}$]) self-assembled into spherical polymersomes in water (Fig. 1-27A and 1-27D). To induce the configurational change of H1 embedded in the discrete hydrophobic block, the self-assembled polymersomes were irradiated with 405 nm light for 2 h at room temperature. Upon blue light irradiation, the polymersomes of **BCP1** changed shape from spherical to flower-like structures due to the formation of numerous buds on the surface of the polymersomes (Fig. 1-27B and 1-28). In contrast, the polymersomes of **BCP2** did not undergo shape transformation upon irradiation (Fig. 1-27E and 1-29). The absence of shape transformation was also observed from the DLS experiments, which only showed a slight difference in the average diameter of self-assembled structures upon irradiation (Fig. 1-26B). To investigate the reversibility of the shape transformation of the polymersomes of **BCP1**, the dispersion of **BCP1** containing shape-transformed polymersomes was irradiated with UV light (365 nm) for 2 h at 25 °C. TEM analysis revealed that the buds formed at the circumference of the polymersomes of **BCP1** were detached from the polymersomes upon UV light irradiation, resulting in the formation of small polymersomes (Fig. 1-27C).

This observation was confirmed by cryogenic transmission electron microscopy (cryo-TEM). The cryo-TEM images of the self-assembled structures show that **BCP1** self-assembled into round vesicles (Fig. 1-4A). The polymersomes underwent shape transformation and formed flower-like structures upon irradiation with 405 nm light for 2 h (Fig. 1-4B), which subsequently were broken into smaller polymersomes upon irradiation with UV light (Fig. 1-4C). The size of the self-assembled nanoparticles was determined from the hydrodynamic diameter of the nanoparticles suspended in water, which was measured by dynamic light scattering (DLS) analysis. The average diameter of the **BCP1** nanoparticles was 534 nm initially, decreased upon blue-light irradiation followed by an increase to 612 nm upon UV light irradiation. We reasoned that this change arose from the shape transformation of the polymersomes of **BCP1** as observed by cryo-TEM (Fig. 1-26A).

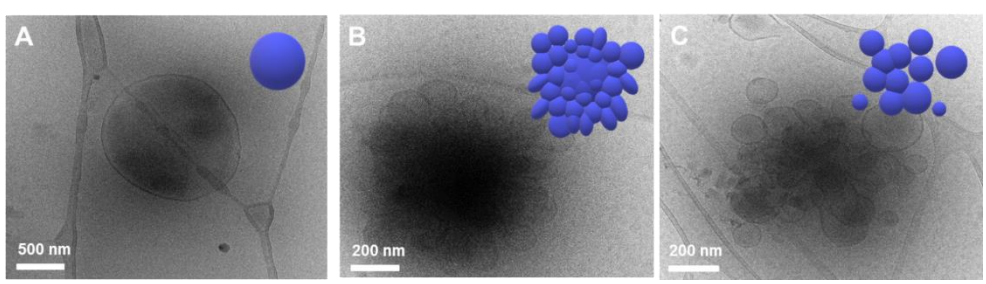

Fig. 1-4 Cryo-TEM images and 3D graphic representations of self-assembled structures of PEG550-*b*-[$OPLA_8$-H1-$OPLA_9$] under different light sources. The morphologies were observed (A) before and (B) after blue-light irradiation, followed by (C) UV light irradiation.

Shape transformations of BCP3 and BCP4 containing PEG1000 as hydrophilic blocks.

The morphological transition of **BCP1** polymersomes under irradiation due to the isomerization of H1 embedded in the discrete OPLA block was irreversible even when the polymersomes were irradiated with a different wavelength of light. We attributed the irreversible shape change to the insufficient colloidal stability of the **BCP1** polymersomes having a short PEG chain (M_n = 550 Da). Therefore, we introduced higher molecular-weight PEG as a hydrophilic block and synthesized **BCP3** and **BCP4** having hydrophilic PEG blocks (M_n = 1000 Da, $Đ$ = 1.02) and the same discrete OPLA blocks as that present in **BCP1** and **BCP2**. When self-assembled by the same co-solvent method as that used in the case of **BCP1** and **BCP2**, **BCP3** (PEG1000-*b*-[$OPLA_8$-H1-$OPLA_9$]), self-assembled into a mixture of spherical and elongated polymersomes (Fig. 1-5A and 1-30A), while **BCP4** (PEG1000-*b*-[H1-$OPLA_{17}$]), self-assembled into sponge-phase particles (Fig. 1-5D and 1-31A). Upon irradiation with 405 nm light, the photoswitch underwent *Z* to *E* isomerization, and the **BCP3** polymersomes underwent shape change to urchin-like vesicles with small buds protruding from the bilayer membrane (Fig. 1-5B, 1-30B and 1-32). As expected, these polymersomes regained their initial shape when the photoswitch in the OPLA block underwent *E* to *Z* isomerization after irradiation with UV light for 2 h (Fig. 1-5C and 1-30C). The average diameter of the **BCP3** nanoparticles decreased from 752 nm to 638 nm upon blue-light irradiation followed by an increase upon UV light irradiation, indicates similar trend to that observed in **BCP1** (Fig. 1-30D). In contrast, the **BCP4** polymersomes did not undergo any shape transformation (Fig. 1-5E and 1-31).

When the BCPs are irradiated with 405 nm light, the H1 units in both **BCP3** and **BCP4** undergo E-Z isomerization; this resulted in a distinct shape transformation in

the case of **BCP3**, while no visible shape change was observed in the case of **BCP4** although both **BCP3** and **BCP4** have the same molecular weights. This indicates that controlling the position of the photoswitch in the BCP is critical for shape transformation. When H1 is located at the middle of the hydrophobic chain, the self-assembled nanostructures underwent significant shape transformation due to the photoisomerization of the photoswitch. In contrast, no shape change was observed when H1 was located at the junction of the hydrophilic and hydrophobic blocks.

A plausible explanation could be that the trans-cis isomerization of the photoswitch in the middle of the hydrophobic OPLA block would introduce a kink, which causes the conformational change of the hydrophobic chain (Fig. 1-3). This change might lead to the increase of the interfacial area of the compartmentalizing membrane of the polymersome. Assuming the constant volume of the internal water-filled compartment, the membrane would develop protrusion to compensate the increased interfacial area, which results in the shape transformation of polymersomes.

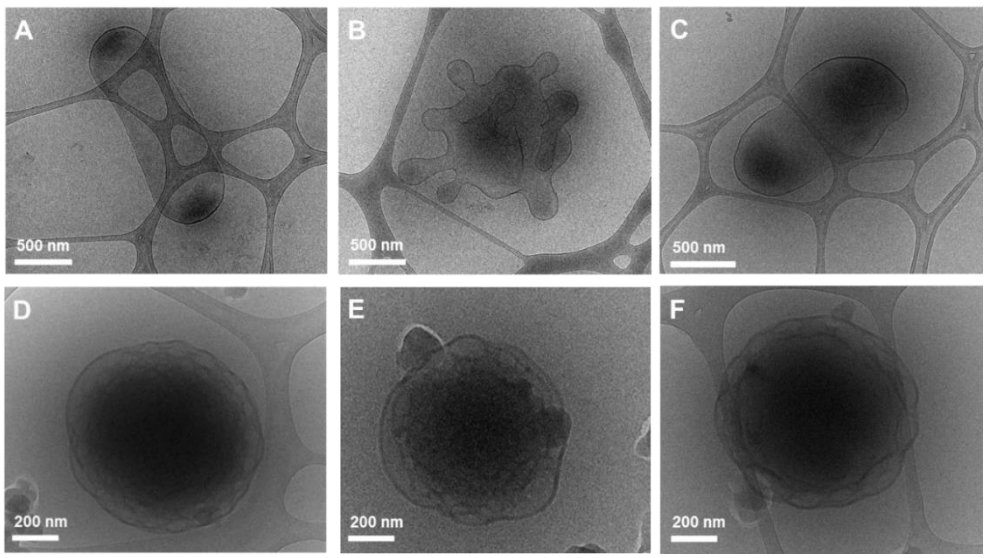

Fig. 1-5 Cryo-TEM images of self-assembled structures of (A−C) PEG1000-*b*-[$OPLA_8$-H1-$OPLA_9$] and (D−F) PEG1000-*b*-[H1-$OPLA_{17}$] under different light sources. The morphologies were observed (A and D) before and (B and E) after blue light irradiation, followed by (C and F) UV light irradiation.

2) Effect of the number of hydrazone photoswitches in the BCP backbone

We found that the **BCP3** polymersomes underwent shape transformation when H1 was located at the center of the hydrophobic chain in **BCP3** (PEG1000-*b*-[$OPLA_8$-H1-$OPLA_9$]). The presence of H1 within the hydrophobic core of the self-assembled BCP that underwent photo-induced configurational change resulted in a change in the bilayer membrane of the polymersomes. Therefore, we investigated the effect of the number of H1 in the hydrophobic chain on the extent of shape transformation. For this, we synthesized of **BCP5** composed of a hydrophilic PEG

block and hydrophobic blocks ($Đ$ = 1) with two H1 units (Scheme 1-9 and Fig. 1-6). **BCP5** comprising discrete hydrophobic chains with multiple H1 units and PEG hydrophilic blocks with a molecular weight (M_n) of 1000 was characterized by ^{1}H NMR spectroscopy and MALDI-TOF spectrometry (Fig. 1-24 and 1-25); the results are summarized in Table 1-1.

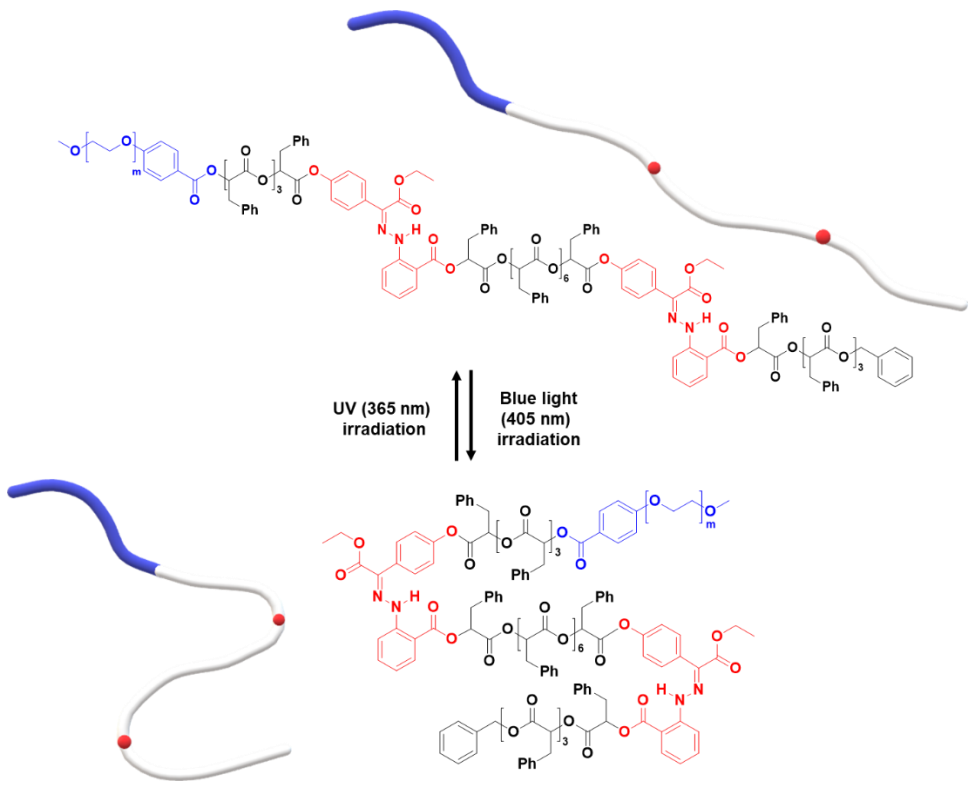

Fig. 1-6 Photo-induced isomerization of two photoswitches in the hydrophobic chain of PEG1000-*b*-[OPLA$_4$-H1-OPLA$_8$-H1-OPLA$_4$].

Shape transformations of BCP5 containing two photoswitches in the hydrophobic chain under different light sources.

BCP5 was self-assembled by a modified co-solvent self-assembly method, in which distilled water was added until the H_2O:acetone ratio reached 1:2. The high acetone content imparts fluidity to the sample with higher crystallinity due to an increase in the number of photoswitches. The induced configurational change in H1 was confirmed by the shape transformation of the polymersomes as observed by TEM. The prepared **BCP5** (PEG1000-*b*-[$OPLA_4$-H1-$OPLA_8$-H1-$OPLA_4$]) self-assembled into spherical vesicles (Fig. 1-7A). The average diameter of the polymeric vesicles was 890 nm, which decreased upon blue-light irradiation corresponding to the enhanced change in the shape of the nanostructures observed by TEM (Fig. 1-34).

The self-assembled nanoparticles were irradiated with 405 nm light for 2 h at room temperature. After blue-light irradiation, the polymeric vesicles formed elongated structures (Fig. 1-7B and Fig. 1-33) with an average diameter of 520 nm, which indicates that the *Z-E* isomerization of the multiple H1 units enhanced the shape transformation effect as confirmed by the significant decrease in the hydrodynamic diameter of the nanoparticles. Upon UV light irradiation, the elongated structures transformed into a mixture of round and tubular vesicles (Fig. 1-7C). The remarkable reversibility of shape transformation because of which most of the particles regained their initial morphology, indicates that the reversible photoisomerization of the hydrazone-based photoswitches enhanced with an increase in the number of photoswitches in the BCP backbone. This in turn affected the extent of shape transformation of the nanostructures.

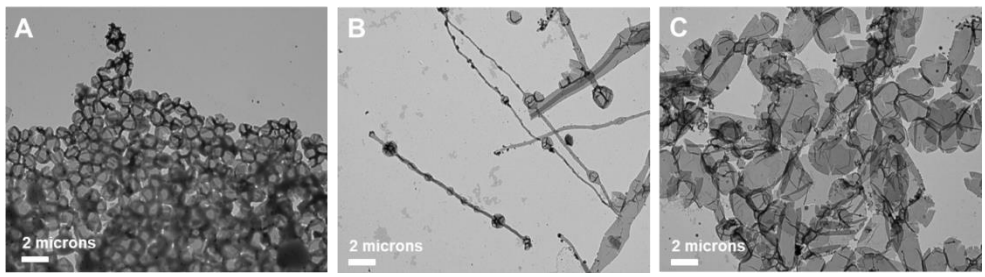

Fig. 1-7 TEM images of self-assembled structures of PEG1000-*b*-[OPLA$_4$-H1-OPLA$_8$-H1-OPLA$_4$] under different light sources. The morphologies were observed (A) before and (B) after blue-light irradiation, followed by (C) UV light irradiation. The PEG1000-*b*-[OPLA$_4$-H1-OPLA$_8$-H1-OPLA$_4$] samples were treated with phosphotungstic acid solution for negative staining.

Further, the pristine samples were irradiated under blue light for different irradiation times (15, 30, and 120 min) at room temperature. Fig. 1-8 shows the TEM images of the irradiated self-assembled polymer vesicles. After 15 min of blue light irradiation, spherical vesicles formed with few elongated structures (Fig. 1-8B), which indicates the limited *Z* to *E* isomerization of H1 embedded in **BCP5**. Furthermore, the number of elongated structures increased with increasing irradiation time (Fig. 1-8C and 1-8D), which indicates an increase in the concentration of *E*-isomer. The ratio of the elongated structures to the spherical vesicles increases as the ratio of *Z*- isomers to *E*- isomers varies with irradiation time.

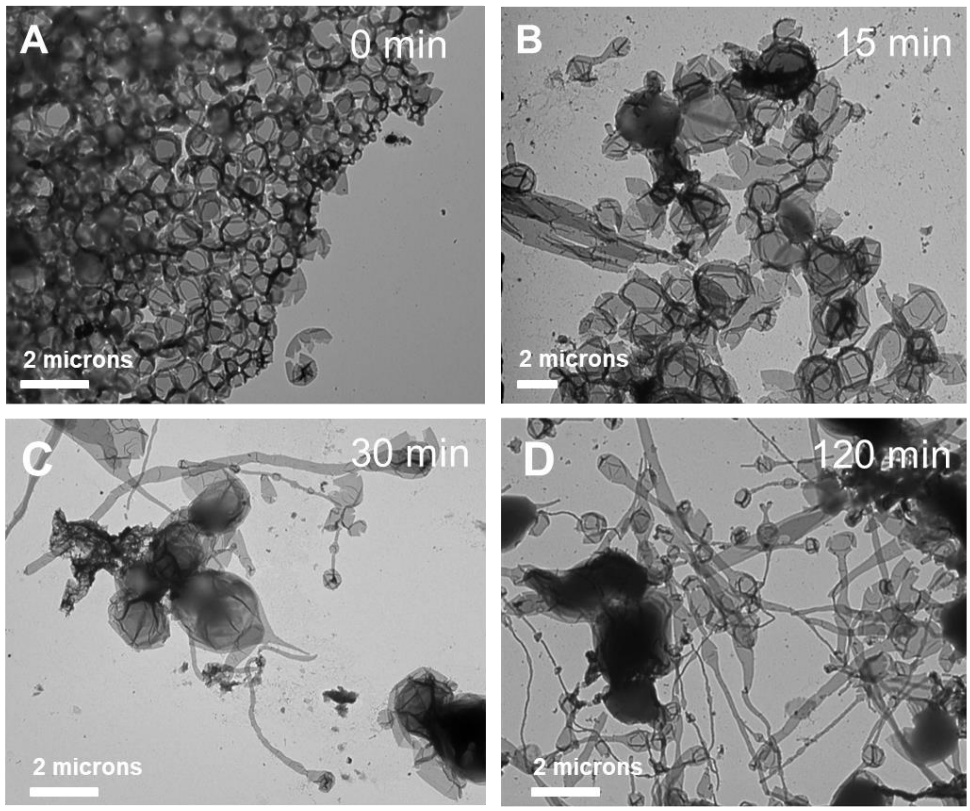

Fig. 1-8 TEM images of self-assembled structures of PEG1000-*b*-[OPLA$_4$-H1-OPLA$_8$-H1-OPLA$_4$] under blue-light irradiation at different irradiation times. The morphologies were observed (A) before blue light irradiation and, after (B) 15 min, (C) 30 min, and (D) 120 min of blue light irradiation. The PEG1000-*b*-[OPLA$_4$-H1-OPLA$_8$-H1-OPLA$_4$] samples were treated with phosphotungstic acid solution for negative staining.

1.4 CONCLUSION

In summary, we synthesized BCPs composed of hydrophilic PEG blocks and OPLA blocks containing hydrazone-based photoswitches in specific positions. The BCPs self-assembled into nanostructures via a cosolvent self-assembly method. We found that the configurational change of the hydrazone-based photoswitches can be translated to macroscopic actuation such as the shape transformation of the self-assembled nanoparticles. The nanoparticles constructed with BCPs with the hydrazone-based photoswitch embedded at the middle of the hydrophobic OPLA chains exhibited dramatic membrane deformation, with reversible shape transformation from polymeric vesicles to urchin-like structures. In contrast, the self-assembled nanostructures of BCPs with the hydrazone-based photoswitches embedded at the junction of the hydrophilic and hydrophobic blocks did not undergo shape transformation upon irradiation with different light sources. This indicates that the position of the switch in the hydrophobic OPLA chain is a decisive factor that determines the shape transformation of the nanoparticles driven by the light-induced configurational change of the hydrazone-based photoswitches. Furthermore, with an increase in the number of photoswitches embedded in the OPLA chains, the extent of shape transformation is significantly enhanced. The on-demand actuation of our system can contribute significantly to the design and development of BCPs for the fabrication of polymersomes for a wide range of potential applications including delivery systems for cargo molecules.

1.5 Experimental Section

1. Materials and methods

General

Unless otherwise noted, all reagents and chemicals were purchased from Sigma Aldrich, Alfa Aesar and TCI and used as received. Dichloromethane (CH_2Cl_2) was distilled over CaH_2 under N_2. All reactions were performed under an inert atmosphere unless otherwise stated.

Methods

^{1}H and ^{13}C NMR spectra were recorded on Agilent 500-MR DD2 Magnetic Resonance System and Varian/Oxford AS-500 using CD_2Cl_2 and $CDCl_3$ as solvents and internal standards. Molecular weights and dispersity D of polymers and block copolymers were measured by Agilent 1260 Infinity gel permeation chromatography (GPC) system equipped with a PL gel 5 μm MiniMIX-D column (Agilent Technologies) and differential refractive index detectors. THF was used as an eluent with a flow rate of 1 mL min^{-1} at 30 °C. A PS standard kit (Agilent Technologies) was used for calibration. Matrix-assisted laser desorption/ionization time-of-flight mass spectrometry (MALDI-TOF-MS) was performed on Bruker Ultraflex II TOF/TOF mass spectrometer equipped with a nitrogen laser (335 nm). The analytical sample was prepared by mixing a THF solution of an analyte with a THF solution of 2-(4-Hydroxyphenylazo)benzoic acid (HABA) matrix. Cryogenic transmission electron microscopy (cryo-TEM) images were taken from JEM-1400 (JEOL) operating at 120 kV. The cryo-TEM experiments were performed with a thin film of aqueous sample solution (5 μL) transferred to a lacey supported grid

(copper, 200 mesh, EM science) by the plunge-dipping method. The thin aqueous films were prepared at ambient temperature and with a humidity of 97–99% within custom-built environmental chamber in order to prevent water evaporation from the sample solution. The excess liquid was blotted with filter paper for 1–2 s, and the thin aqueous films were rapidly vitrified by plunging them into liquid ethane (cooled by liquid nitrogen) at its freezing point. Conventional TEM was performed on a Hitachi 7600 operating at 100 kV. Specimens were prepared by placing a drop of the sample solution on a carbon-coated Cu grid (200 mesh, EM science) and then air-drying the grid overnight. If necessary, specimens were prepared by premixing of dilute polymer solution (0.1 mg/mL) and phosphotungstic acid solution (2%) in a 10 : 1 volume ratio, and a drop of the premixed solution was placed on a carbon-coated Cu grid (200 mesh, EM Science). Dynamic light scattering (DLS) was performed on Malvern Zetasizer Nano-S. The dialyzed self-assembled polymer solution was diluted with water and an aliquot of 4 mL of the diluted solution was transferred into a plastic cuvette for measurement. Intensity data from each sample were collected in three replicates at 25 °C.

2. Preparation of hydrazone-based photo-switch

Hydrazone-based photo-switch (THP-H1-COOH) was synthesized by following the previously reported procedure.[40]

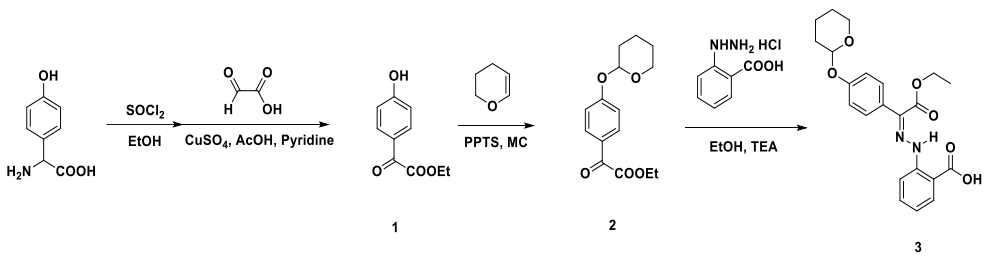

Scheme 1-3 Synthesis of hydrazone-based photo-switch.

THP-H1-COOH (3). It is synthesized in multi-gram quantity by following the literature methods.

^{1}H NMR (500 MHz, $CDCl_3$) δ 13.67 (s, 1H), 8.02 (dd, J=8.0, 1.5 Hz, 1H), 7.94 (d, J=8.0 Hz, 1H), 7.64 (d, J=9.0 Hz, 2H), 7.54 (t, J=8.5 Hz, 1H), 7.07 (d, J=9.0 Hz, 2H), 6.95 (t, J=8.0 Hz, 1H), 5.48-5.47 (m, 1H), 4.45 (q, J=7.0 Hz, 2H), 3.95-3.90 (m, 1H), 3.64-3.61 (m, 1H), 2.05-2.00 (m, 1H), 1.90-1.87 (m, 2H), 1.70-1.55 (m, 3H), 1.39 (t, J=7.0 Hz, 3H) ppm; ^{13}C NMR (125 MHz, CD_2Cl_2) δ 169.42, 162.97, 157.66, 147.26, 135.57, 132.74, 132.03, 130.08, 130.04(2C), 120.45, 117.49, 116.31(2C), 114.86, 96.84, 62.51, 61.92, 30.73, 25.64, 19.25, 14.41 ppm.

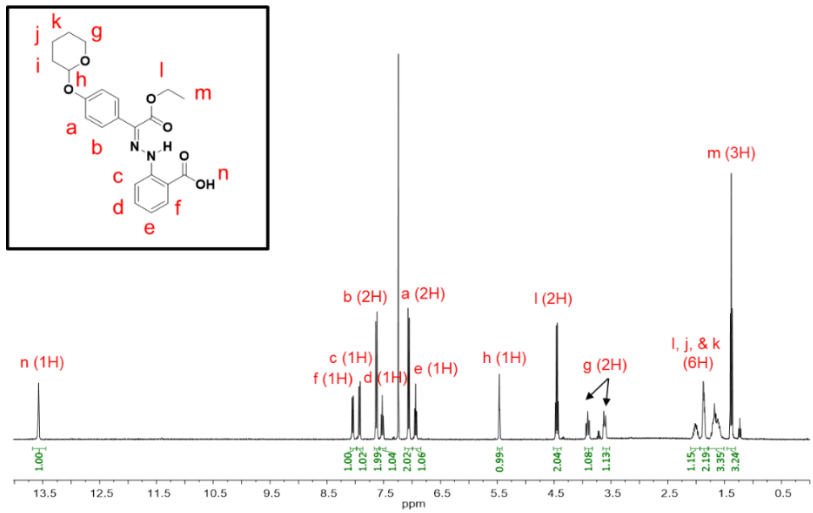

Fig. 1-9 [1]H NMR spectra of hydrazone-based photo-switch (THP-H1-COOH).

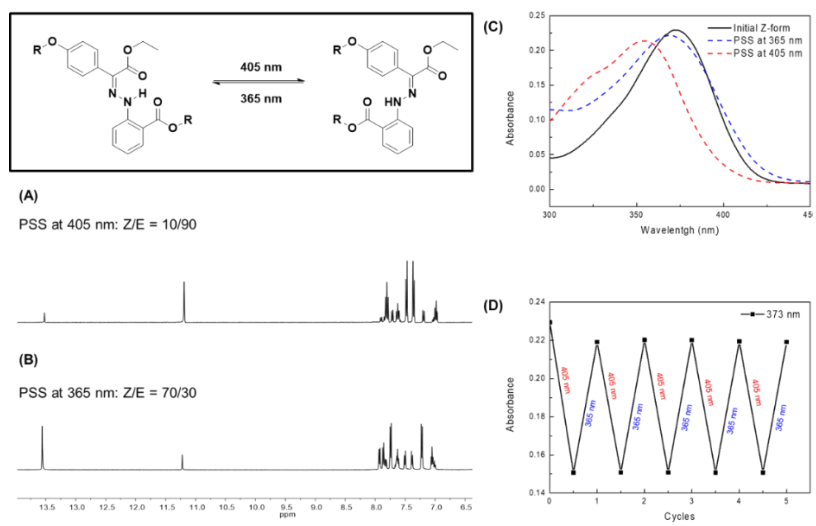

Fig. 1-10 [1]H NMR spectra in DMSO of hydrazone-based photoswitches (A) after 405 nm, followed by (B) 365 nm photoirradiation to reach the PSS. (C) UV-Vis absorption spectra of hydrazone-based photoswitches in DMSO. (D) Switching cycles of hydrazone-based photoswitches in DMSO upon alternating irradiation using 405 nm and 365 nm light sources.

3. Procedure for the convergent growth of oligo(phenyl lactic acid)s

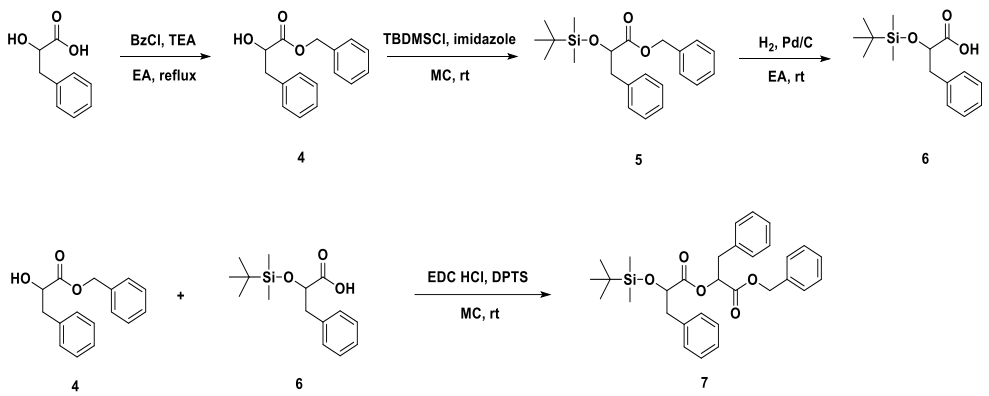

Scheme 1-4 Synthesis of phenyl lactic acid dimer (PLA_2).

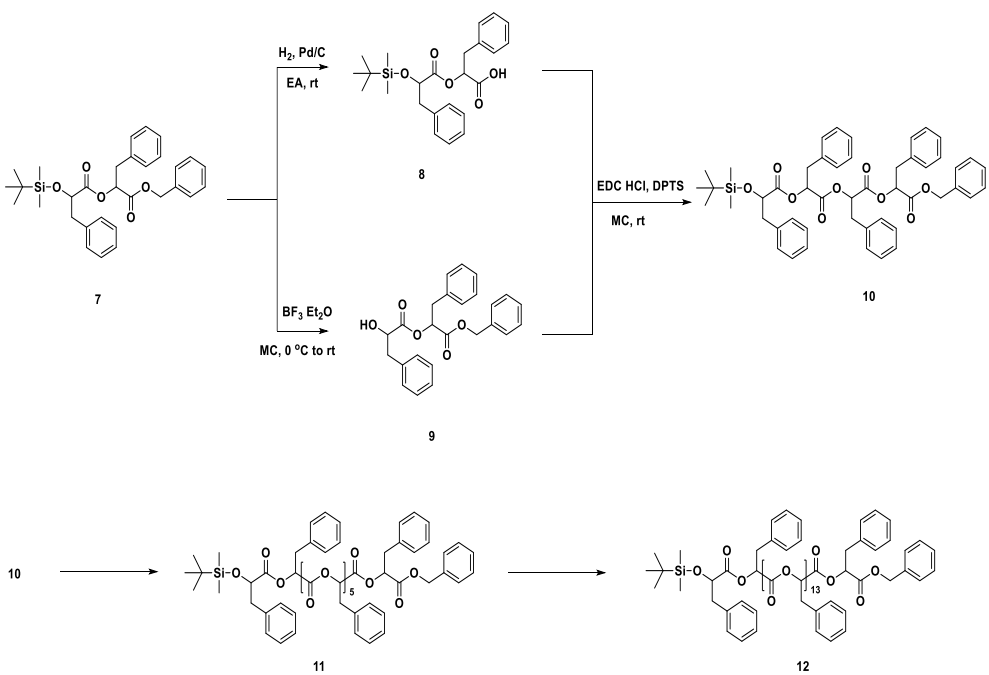

Scheme 1-5 Synthesis of discrete oligo(phenyl lactic acid)s (OPLAs).

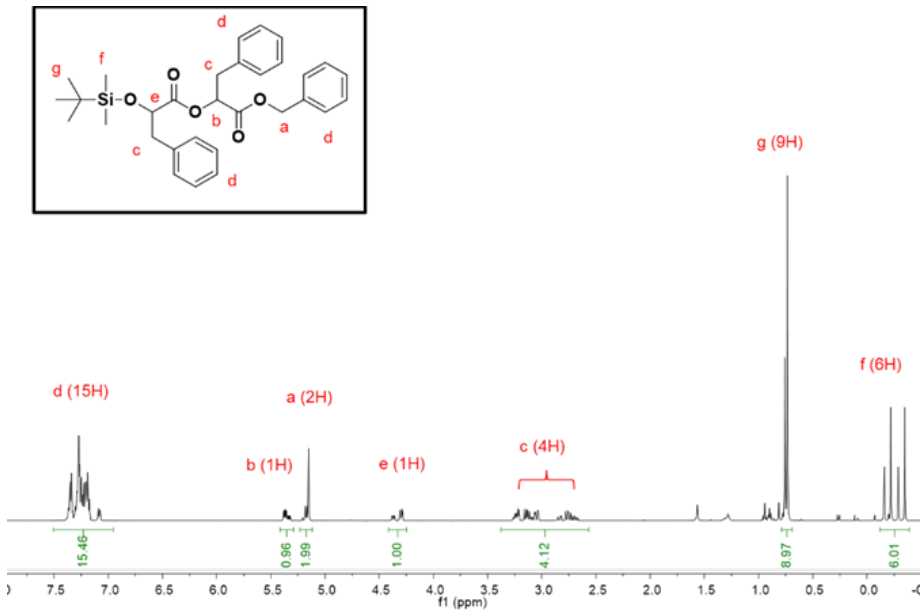

Fig. 1-11 ^{1}H NMR spectra of phenyl lactic acid dimer (PLA_2).

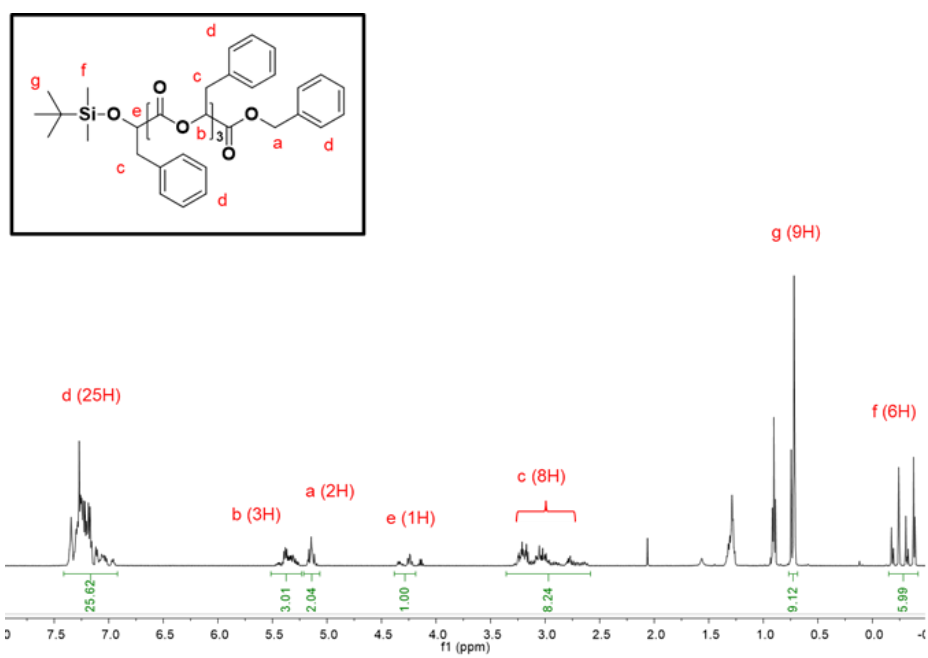

Fig. 1-12 ^{1}H NMR spectra of oligo(phenyl lactic acid) tetramer ($OPLA_4$).

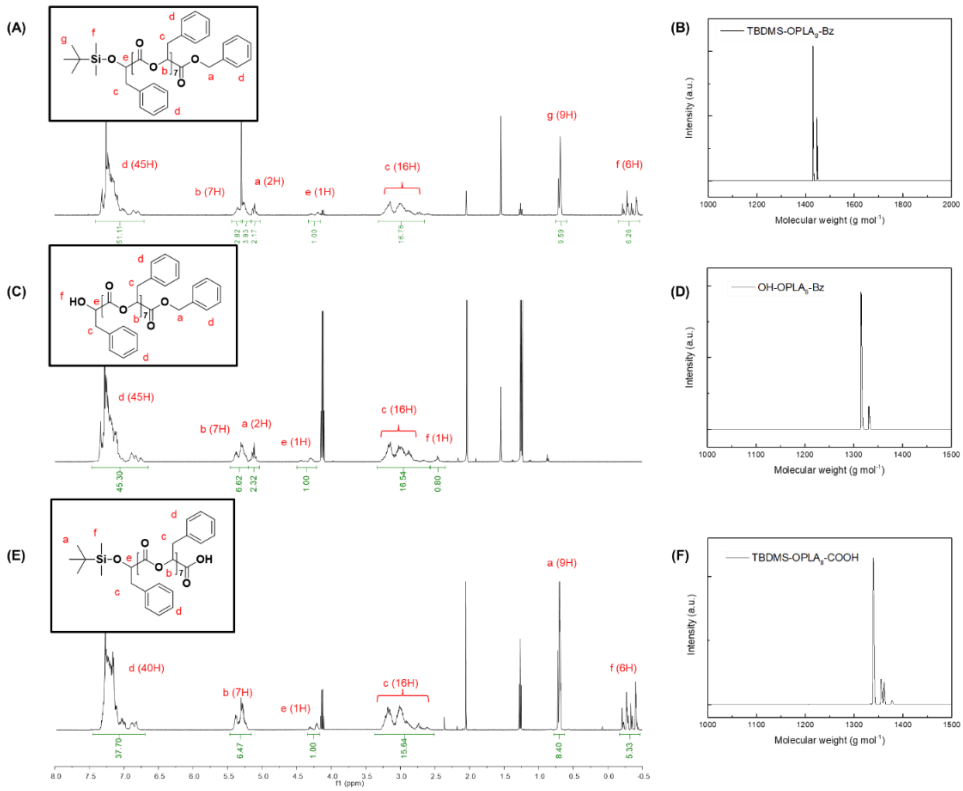

Fig. 1-13 (A, C and E) ^{1}H NMR spectra in $CDCl_3$ and (B, D and F) MALDI-TOF spectra of monodisperse hydrophobic block (TBDMS-$OPLA_8$-Bz), and deprotected (OH-$OPLA_8$-Bz) and (TBDMS-$OPLA_8$-COOH) compounds respectively.

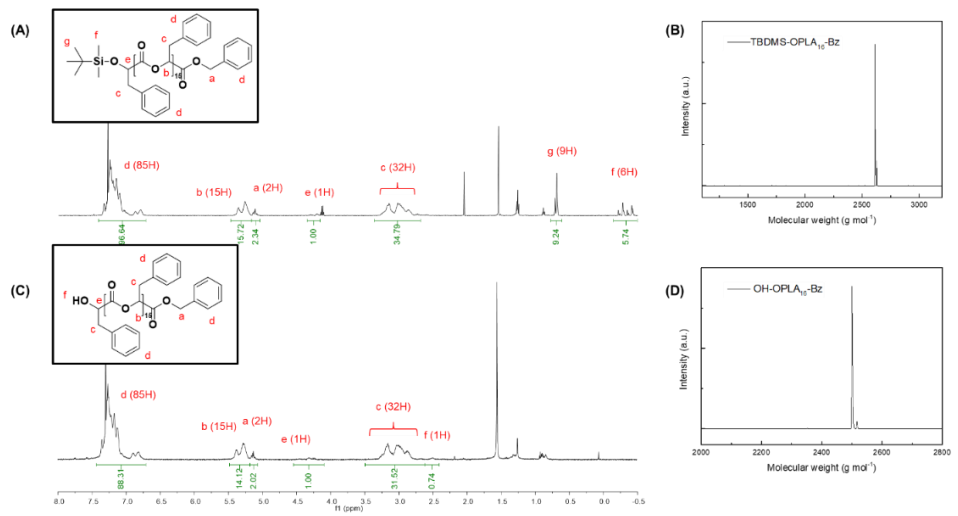

Fig. 1-14 (A and C) ^{1}H NMR spectra in $CDCl_3$ and (B and D) MALDI-TOF spectra of monodisperse hydrophobic block (TBDMS-$OPLA_{16}$-Bz), and deprotected (OH-$OPLA_{16}$-Bz) compound respectively.

$OPLA_{16}$ (12). It is synthesized in multi-gram quantity by following the literature methods. [41]

^{1}H NMR (500MHz, $CDCl_3$): 7.37-7.01 (m, 85H, Ph-H), 5.32 (m, 15H, COO-$CH(CH_3)$C=O), 5.14 (m, 2H, Ph-CH_2-O), 4.30 (ddd, J = 29.2, 9.2, 3.4 Hz, 1H, SiO-$CH(CH_2Ph)$C=O), 2.90 (m, 32H, Ph-CH_2-CH), 0.71 (d, J = 91. Hz, 9H, $(CH_3)_3$C-Si), 0.29 (dd, J = 51.5, 23.9 Hz, 6H, $(CH_3)_3$C-$Si(CH_3)_2$-O) ppm.

4. Synthesis of hydrophilic polyethylene glycol chains

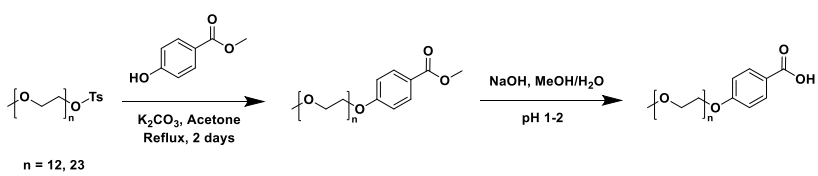

Scheme 1-6 Synthesis of PEGn-COOH.

PEGn-COOH. It is synthesized in multi-gram quantity by following the literature methods.[43,44]

^{1}H NMR (400 MHz, $CDCl_3$) 8.01(d, J=8.4 Hz, 2H), 6.80(s, 2H), 4.11(s, 2H), 3.82(s, 3H), 3.76-3.50(m, -CH_2CH_2O-), 3.36(s, 4H) ppm.

5. Synthesis of block copolymers having hydrazone-based photo-switches

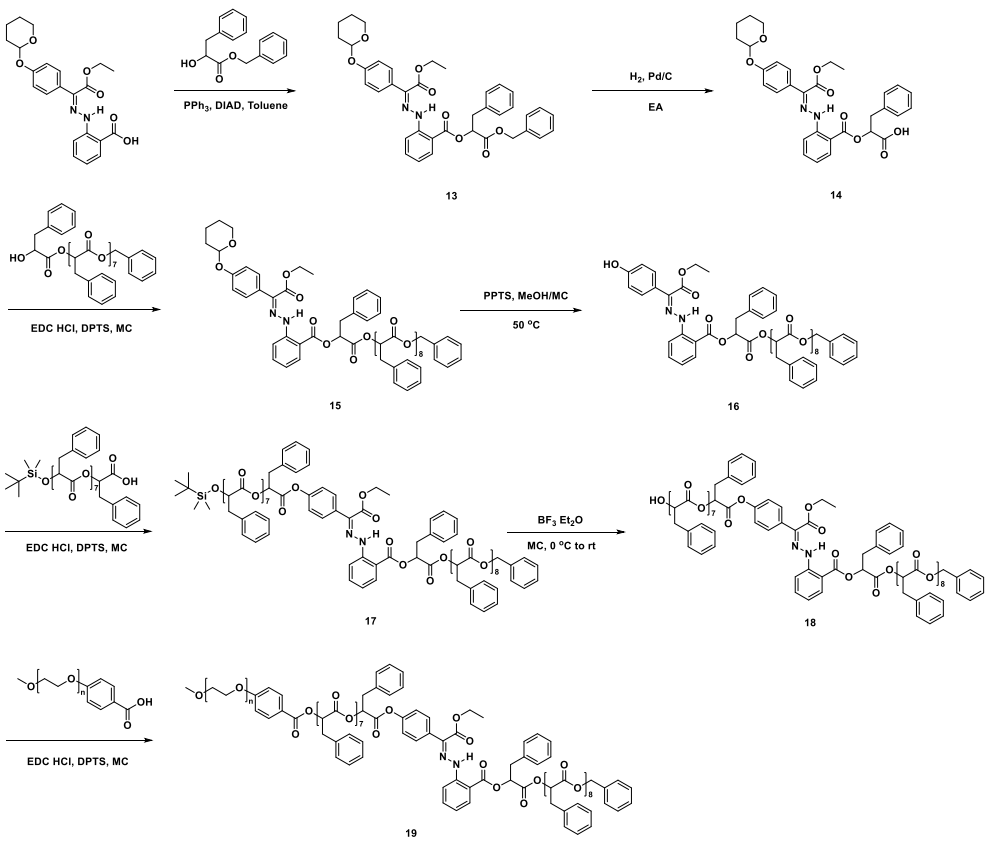

Scheme 1-7 Synthesis of block copolymer having hydrazone-based photo-switches (PEG-*b*-[$OPLA_8$-H1-$OPLA_9$]).

13: DIAD was added to a solution of hydrazone 3, HO-PLA-Bz, and PPh_3 in toluene at 0 °C. The reaction was stirred at room temperature overnight. After removal of the solvent under vacuum, the product was purified by flash column chromatography affording a yellow oil.

14: Palladium on activated charcoal (10% Pd/C) was added to the solution of THP-H1-$OPLA_9$-Bz in EA. The suspension was purged with nitrogen for 15 min. The nitrogen atmosphere was then replaced with hydrogen atmosphere, and the reaction mixture was stirred at room temperature. Upon completion of the reaction, the suspension was filtered through a Celite cake to remove Pd/C. The product was obtained by removing the solvent from the filtrates under reduced pressure.

15: EDC was added to a solution of THP-H1-PLA-COOH (14), HO-$OPLA_8$-Bz, and DPTS in MC at 0 °C. The mixture was stirred at room temperature overnight. After removal of the solvent under vacuum, the product was purified by flash column chromatography affording a yellow oil.

16: A mixture of THP-H1-$OPLA_9$-Bz (15) and PPTS in MC/MeOH was heated to 50 °C and then stirred for 4 h. After removal of the solvent under vacuum, the product was purified by flash column chromatography to afford the *Z*-isomer product.

17: EDC was added to a solution of TBDMS-$OPLA_8$-COOH, HO-H1-$OPLA_9$-Bz, and DPTS in MC at 0 °C. The mixture was stirred at room temperature overnight.

After removal of the solvent under vacuum, the product was purified by flash column chromatography affording a yellow oil.

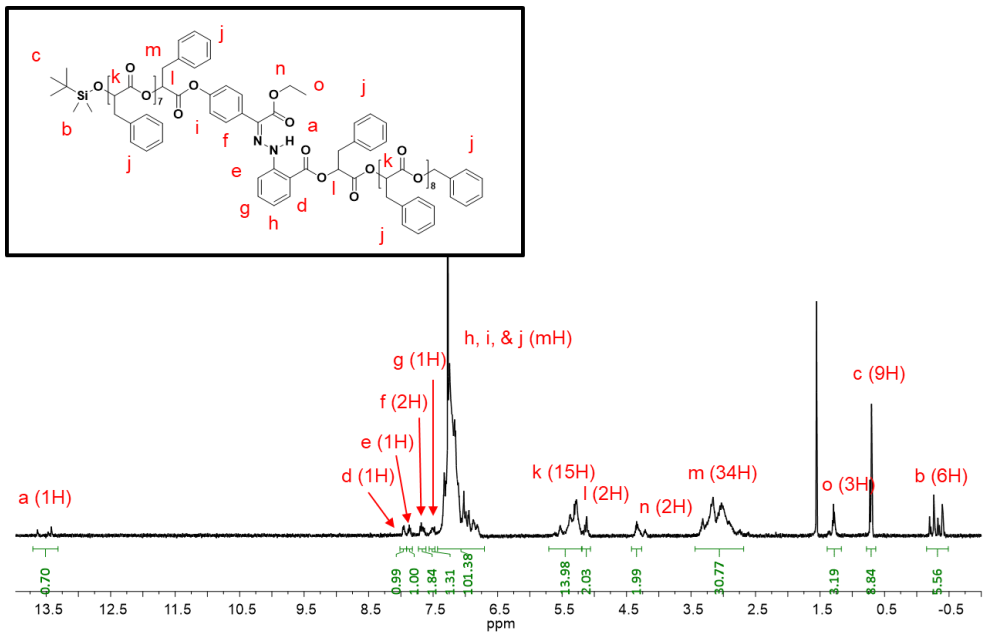

Fig. 1-15 ^{1}H NMR spectra of hydrophobic block (TBDMS-OPLA$_8$-H1-OPLA$_9$-Bz).

18: The hydrophobic chain, TBDMS-OPLA$_8$-H1-OPLA$_9$-Bz (17), was dissolved in dry MC. The solution was cooled to 0 ^{o}C on an ice bath, and boron trifluoride diethyl etherate (BF_3 Et_2O) was added dropwise. The reaction mixture stirred at room temperature for 4 h. Upon completion of the reaction, the reaction was quenched with saturated $NaHCO_3$ followed by dilution with water. The organic layer was separated and washed with brine. The combined organic layer was dried over $MgSO_4$, and the solvent was removed under reduced pressure. The crude product was purified by column chromatography affording a yellow viscous oil.

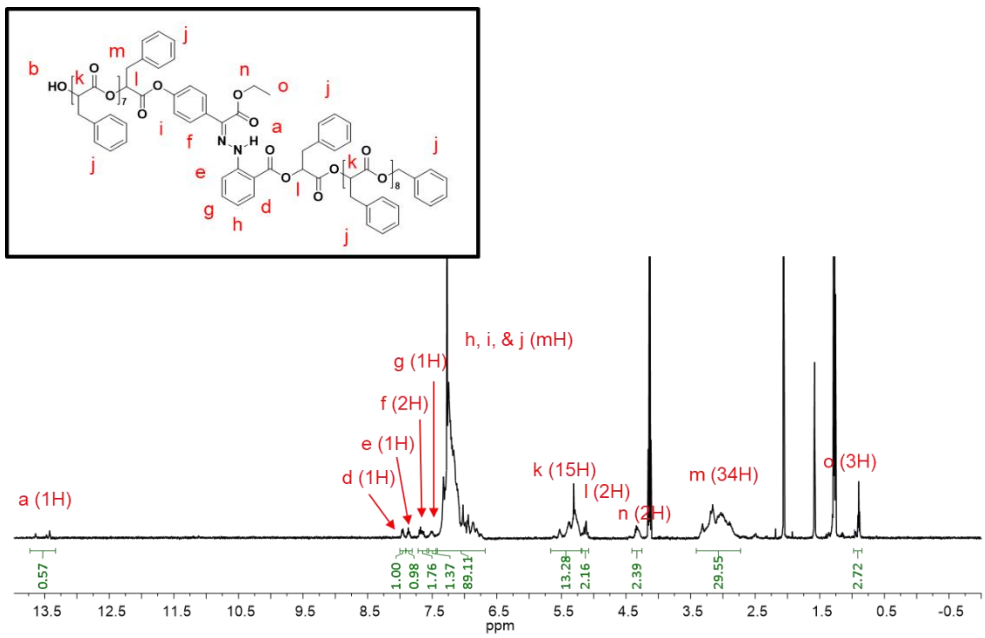

Fig. 1-16 ^{1}H NMR spectra of hydrophobic block (HO-OPLA$_8$-H1-OPLA$_9$-Bz).

19: The deprotected hydrophobic block, HO-OPLA$_8$-H1-OPLA$_9$-Bz (18), and the hydrophilic block, PEG-COOH, were dissolved in dry MC. The mixture was cooled to 0 ºC on an ice bath. To the mixture, 1-(3-dimethylaminopropyl)-3-ethylcarbodiimide hydrochloride (EDC HCl) and DPTS were added. The reaction mixture was stirred overnight at room temperature. Upon completion of the reaction, the reaction mixture was washed with water and brine. The combined organic layer was dried over $MgSO_4$, and the solvent was removed under reduced pressure. The crude product was purified by column chromatography affording a yellow viscous oil.

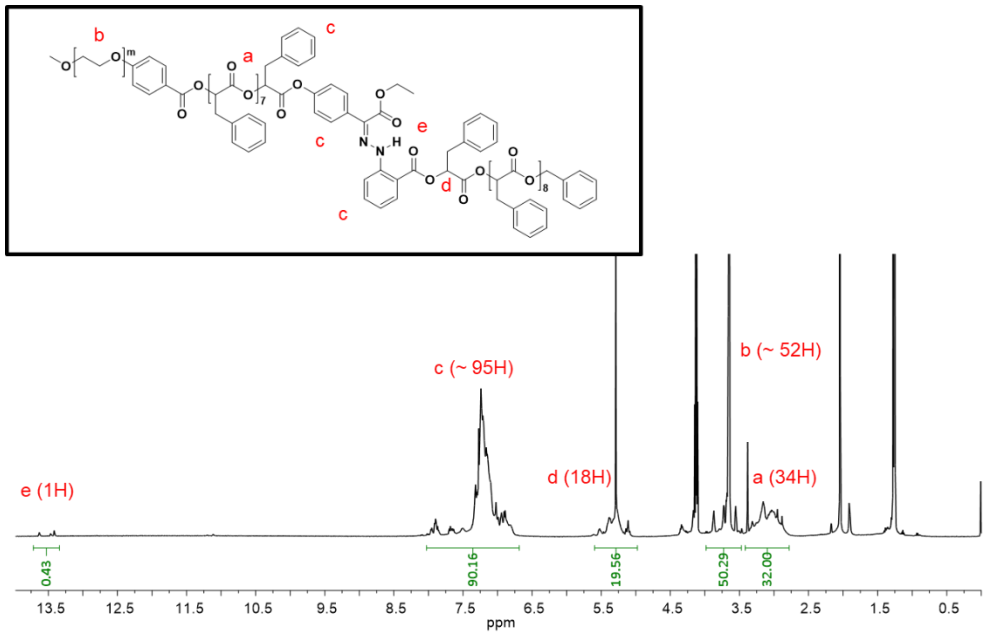

Fig. 1-17 ^{1}H NMR spectra of amphiphilic block copolymer (PEG-*b*-[OPLA$_8$-H1-OPLA$_9$]).

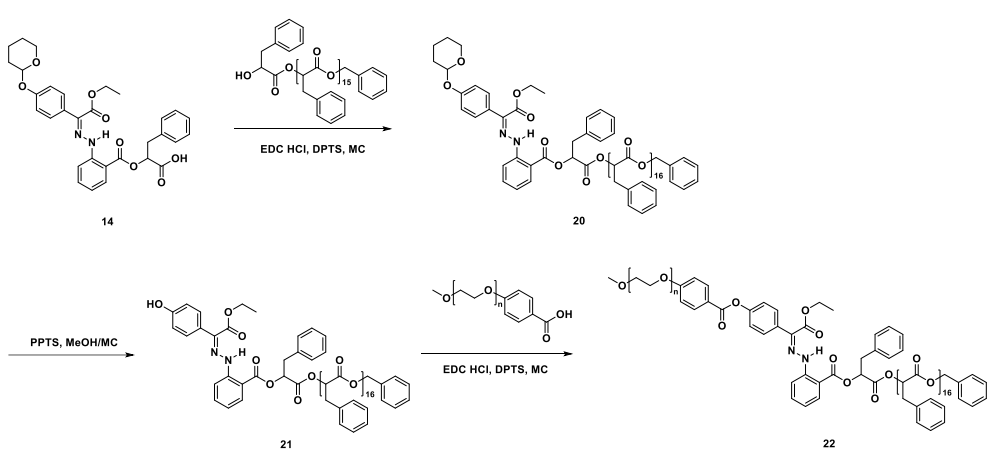

Scheme 1-8 Synthesis of block copolymer having hydrazone-based photo-switches (PEG-*b*-[H1-OPLA$_{17}$]).

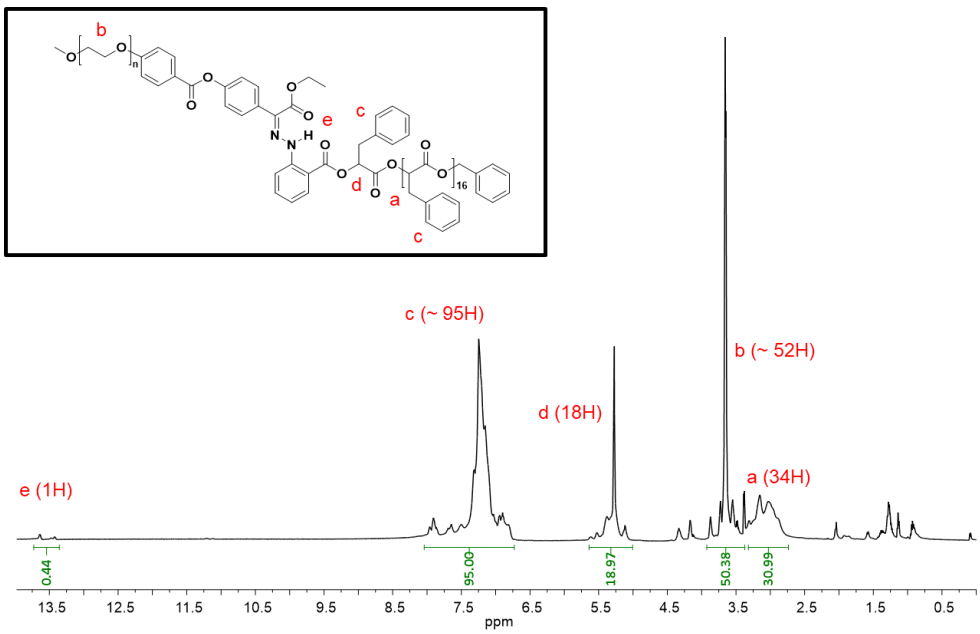

Fig. 1-18 ^{1}H NMR spectra of amphiphilic block copolymer (PEG-*b*-[H1-OPLA$_{17}$]).

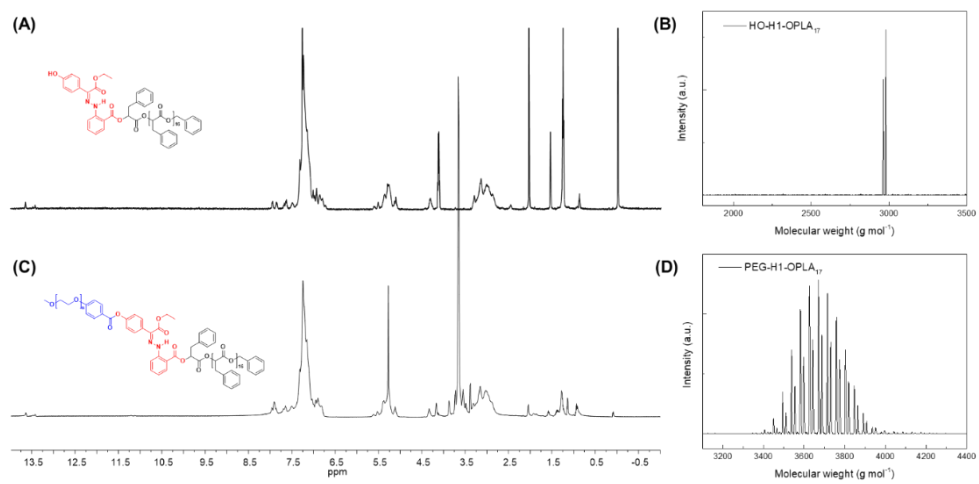

Fig. 1-19 (A and C) ^{1}H NMR spectra in $CDCl_3$ and (B and D) MALDI-TOF spectra of monodisperse hydrophobic block (HO-H1-OPLA$_{17}$) and amphiphilic block copolymer (PEG550-*b*-[H1-OPLA$_{17}$]) respectively.

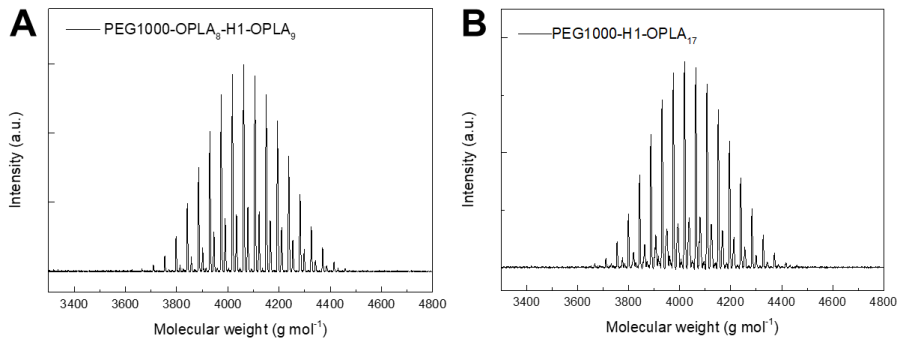

Fig. 1-20 MALDI-TOF spectra of amphiphilic block copolymers (PEG-*b*-[$OPLA_8$-H1-$OPLA_9$] and PEG-*b*-[H1-$OPLA_{17}$]) containing polydisperse hydrophilic block (M_n = 1000).

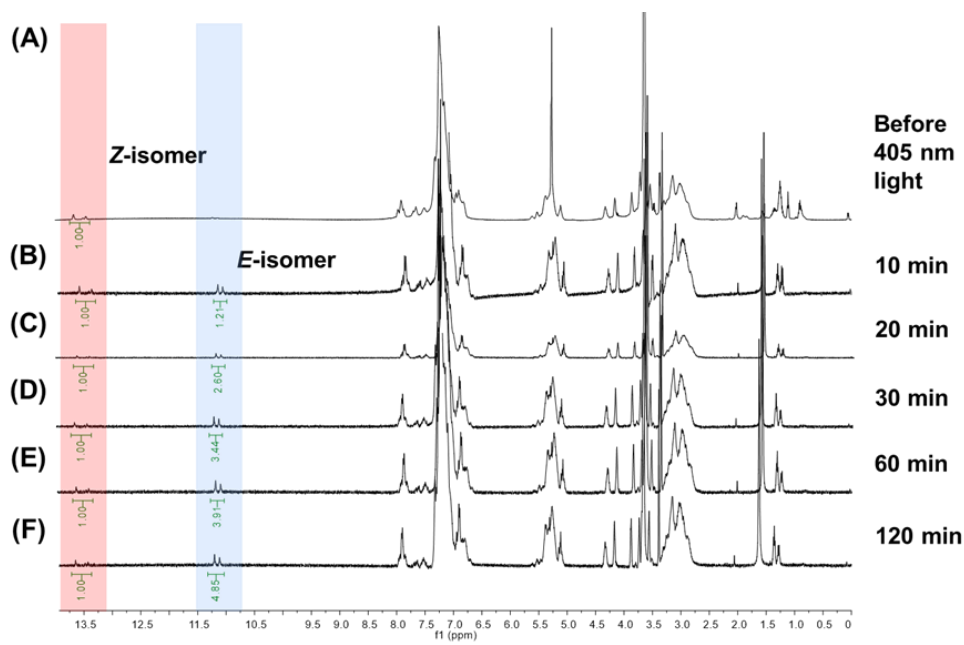

Fig. 1-21 Time-dependent ^{1}H NMR analyses of amphiphilic block copolymer containing hydrazone-based photoswitches (A) before and (B to F) after 405 nm light irradiation.

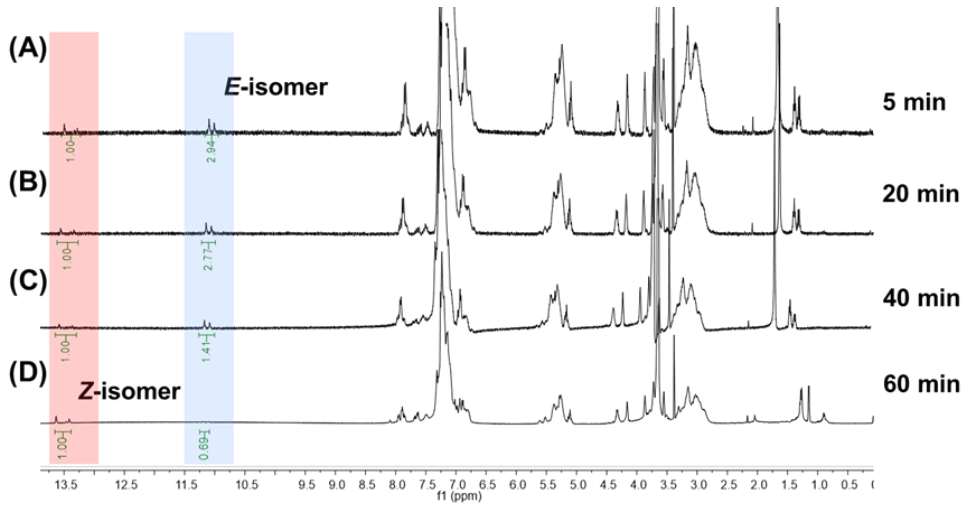

Fig. 1-22 Time-dependent ^{1}H NMR analyses of amphiphilic block copolymer containing hydrazone-based photoswitches (A to D) after 365 nm light irradiation.

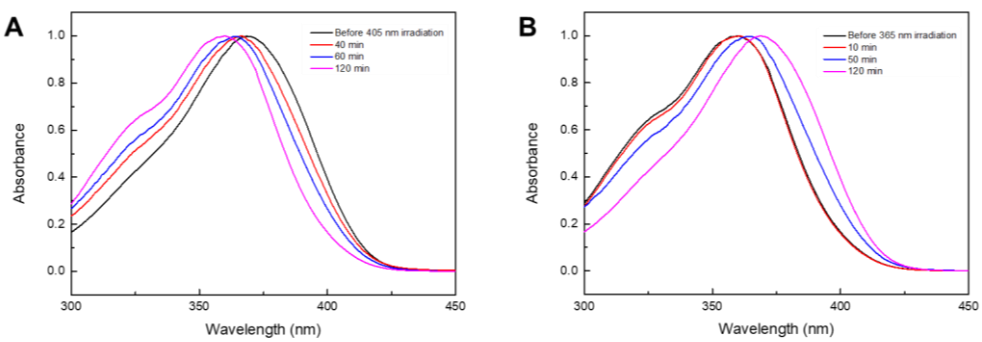

Fig. 1-23 Time-dependent UV-Vis absorption spectra of self-assembled amphiphilic block copolymer containing hydrazone-based photoswitches (A) after 405 nm, followed by (B) 365 nm light irradiation.

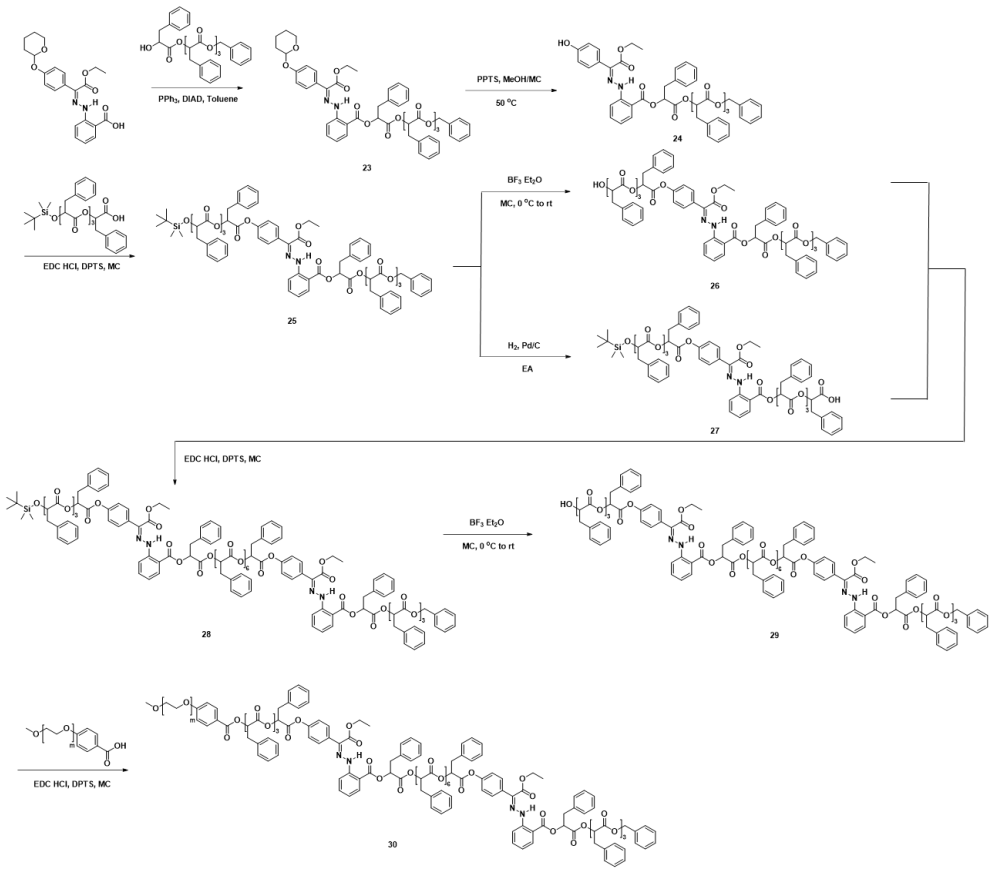

Scheme 1-9 Synthesis of block copolymer having multiple hydrazone-based photo-switches (PEG-*b*-[OPLA$_4$-H1-OPLA$_8$-H1-OPLA$_4$]).

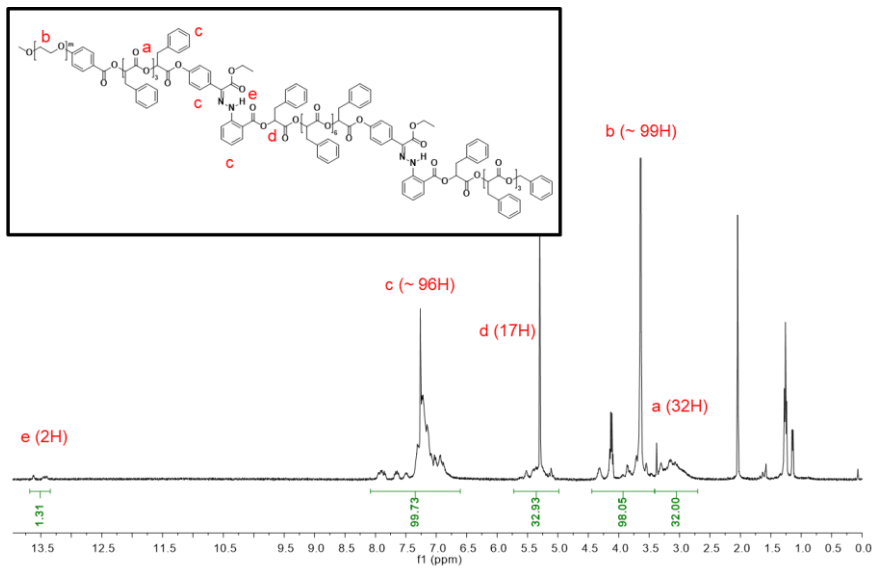

Fig. 1-24 ^{1}H NMR spectra of amphiphilic block copolymer (PEG-*b*-[OPLA$_4$-H1-OPLA$_8$-H1-OPLA$_4$]).

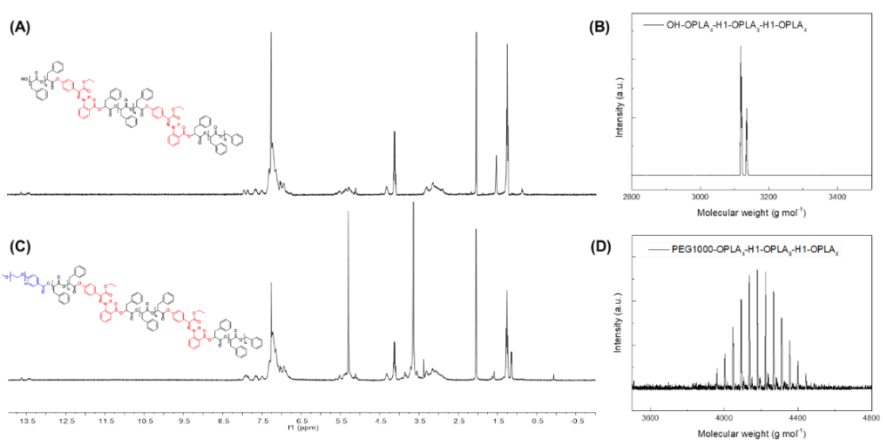

Fig. 1-25 (A and C) ^{1}H NMR spectra in $CDCl_3$ and (B and D) MALDI-TOF spectra of monodisperse hydrophobic block (HO-OPLA$_4$-H1-OPLA$_8$-H1-OPLA$_4$) and amphiphilic block copolymer (PEG1000-*b*-[OPLA$_4$-H1-OPLA$_8$-H1-OPLA$_4$]) respectively.

6. Solution self-assemblies of BCPs via co-solvent method

5 mg of BCPs was dissolved in acetone (1 mL) in a 20 mL capped vial with magnetic stirrer. The solution was stirred for 1 h at room temperature (860 rpm). A syringe pump was calibrated to inject water at a speed of 0.5 mL/h. The vial cap was replaced with a rubber septum, and water was added to the polymer solution over 2 h using a syringe pump with a 6-mL syringe equipped with a steel needle. However, water was added to the polymer solution over 1 h for **BCP5** only. The resulting suspension was subjected to dialysis (molecular weight cutoff 12-14 kDa (SpectraPor, Rancho Dominguez, CA)) against water for 24 h.

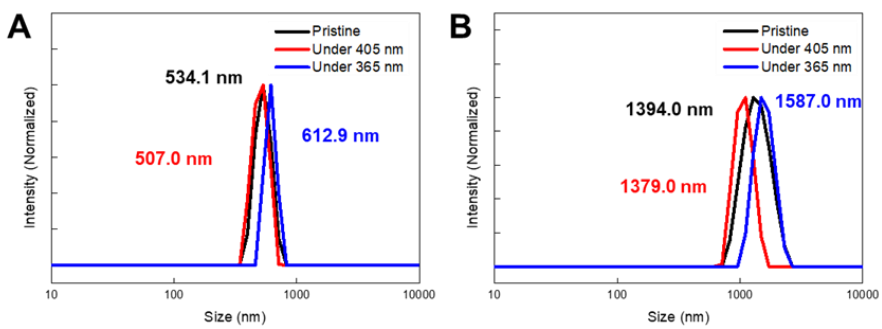

Fig. 1-26 Dynamic light scattering (DLS) analysis of self-assembled structures of (A) PEG550-*b*-[OPLA$_8$-H1-OPLA$_9$] and (B) PEG550-*b*-[H1-OPLA$_{17}$] under different light sources.

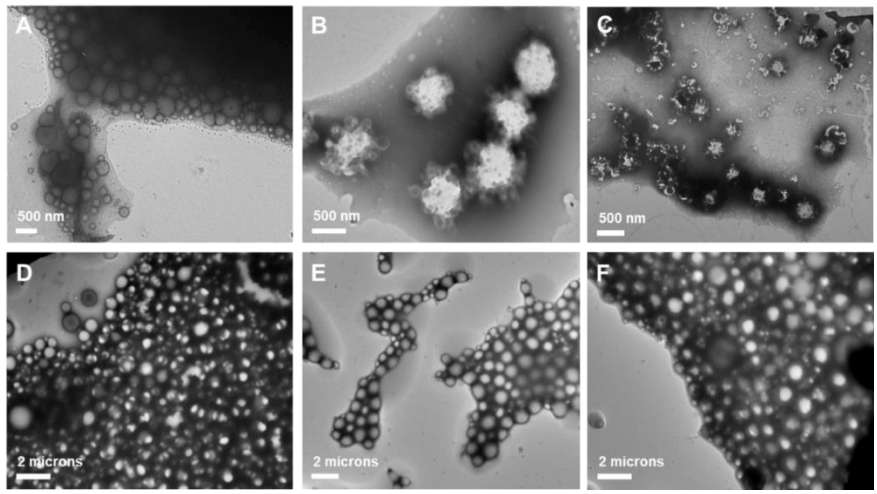

Fig. 1-27 TEM images of self-assembled structures of (A−C) PEG550-*b*-[OPLA$_8$-H1-OPLA$_9$] (D−F) PEG550-*b*-[H1-OPLA$_{17}$] under different light sources. The morphologies were observed (A and D) before and (B and E) after blue-light irradiation, followed by (C and F) UV light irradiation.

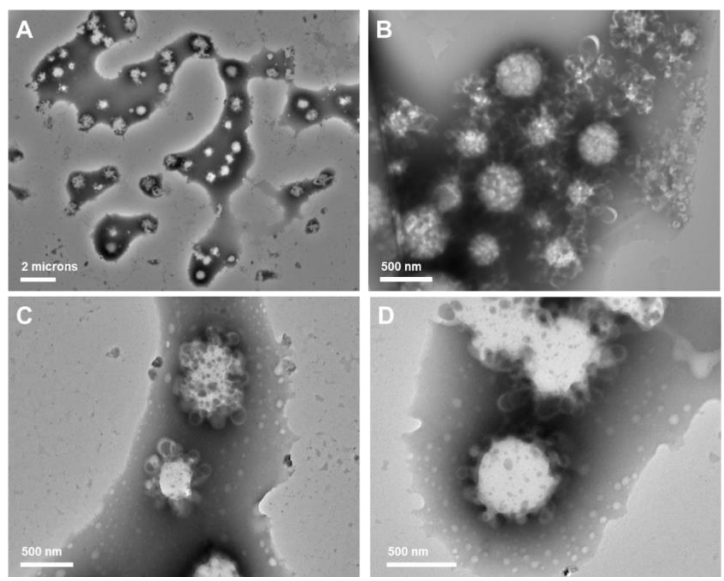

Fig. 1-28 TEM images with different resolutions of flower-like structures. The structures were prepared via the shape transformation of the self-assembled structures of PEG550-*b*-[OPLA$_8$-H1-OPLA$_9$] after blue-light irradiation for 2 h.

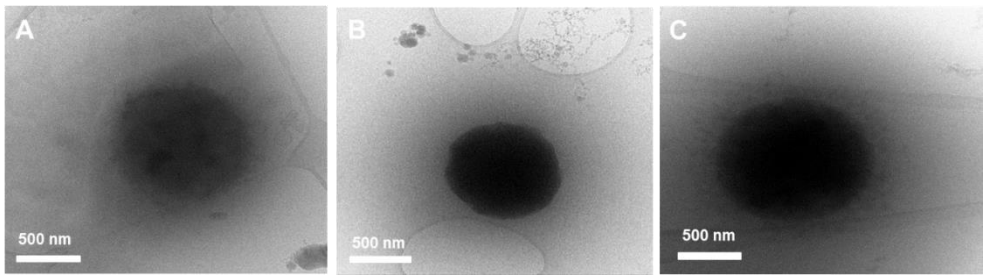

Fig. 1-29 Cryo-TEM images of self-assembled structures of PEG550-*b*-[H1-$OPLA_{17}$] under different light sources. The morphologies were observed (A) before and (B) after blue-light irradiation, followed by (C) UV light irradiation.

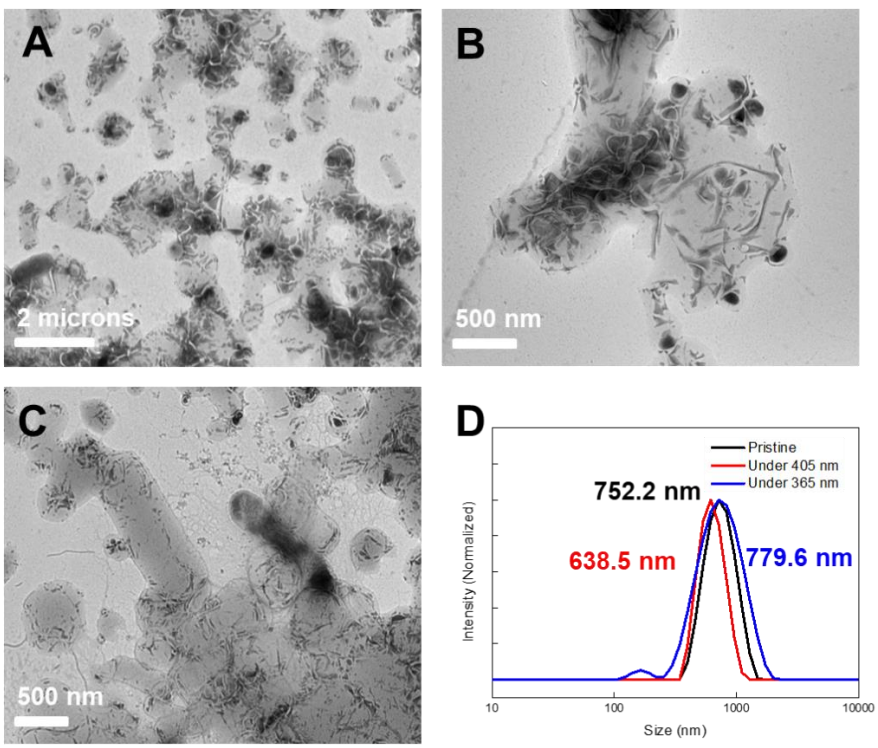

Fig. 1-30 (A−C) TEM images and (D) dynamic light scattering (DLS) analysis of self-assembled structures of PEG1000-*b*-[$OPLA_8$-H1-$OPLA_9$] under different light sources. The morphologies were observed (A) before and (B) after blue-light irradiation, followed by (C) UV light irradiation.

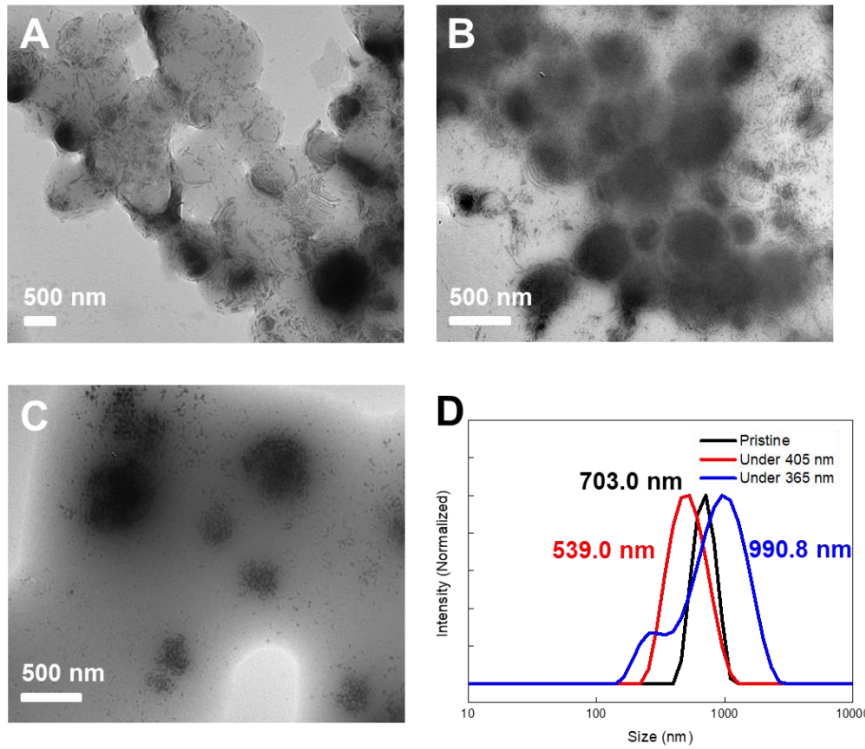

Fig. 1-31 (A−C) TEM images and (D) dynamic light scattering (DLS) analysis of self-assembled structures of PEG1000-*b*-[H1-OPLA$_{17}$] under different light sources. The morphologies were observed (A) before and (B) after blue-light irradiation, followed by (C) UV light irradiation.

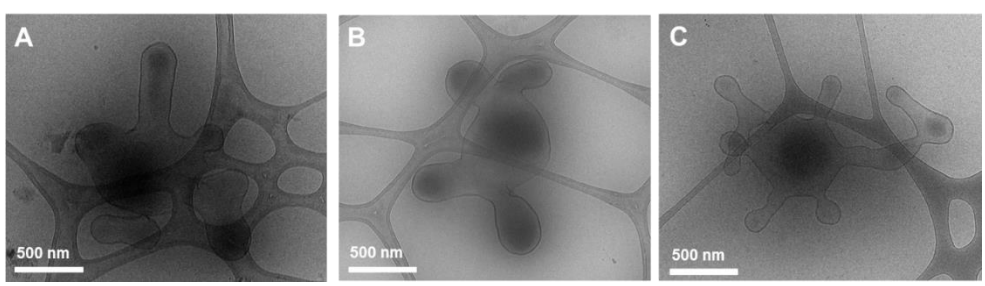

Fig. 1-32 Cryo-TEM images of urchin-like structures of PEG1000-*b*-[OPLA$_8$-H1-OPLA$_9$] after blue-light irradiation.

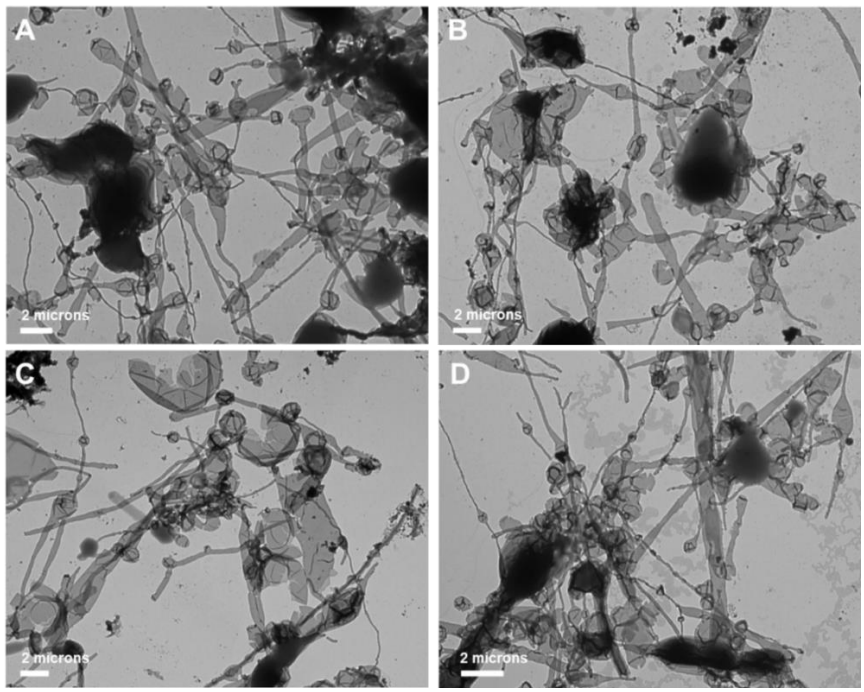

Fig. 1-33 TEM images of elongated structures. The structures were prepared via the shape transformation of the self-assembled structures of PEG1000-*b*-[OPLA$_4$-H1-OPLA$_8$-H1-OPLA$_4$] after blue-light irradiation for 2 h. The structures of PEG1000-*b*-[OPLA$_4$-H1-OPLA$_8$-H1-OPLA$_4$] (A−D) were treated with phosphotungstic acid solution for negative staining.

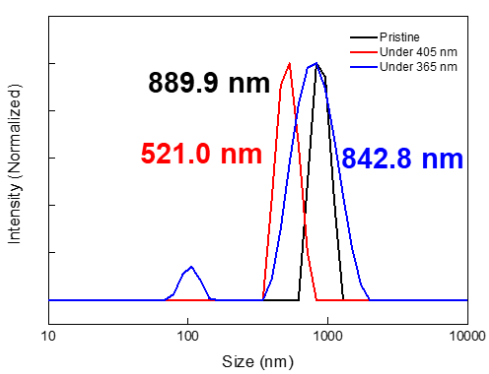

Fig. 1-34 Dynamic light scattering (DLS) analysis of self-assembled structures of PEG1000-*b*-[OPLA$_4$-H1-OPLA$_8$-H1-OPLA$_4$] under different light sources.

1.6 REFERENCES

1 F. Meng, Z. Zhong and J. Feijen, *Biomacromolecules*, 2009, **10**, 197–209.

2 O. Onaca, R. Enea, D. W. Hughes and W. Meier, *Macromol. Biosci.*, 2009, **9**, 129–139.

3 M-H. Li and P. Keller, *Soft Matter*, 2009, **5**, 927–937.

4 X. Hu, Y. Zhang, Z. Xie, X. Jing, A. Bellotti and Z. Gu, *Biomacromolecules*, 2017, **18**, 649−673.

5 Y. Wang and D. S. Kohane, *Nat. Rev. Mater*, 2017, **2**, 17020.

6 U. Kauscher, M. N. Holme, M. Björnmalm and M. M. Steven, *Adv Drug Deliv Rev.*, 2019, **138**, 259−275.

7 S. Hocine, A. Brulet, L. Jia, J. Yang, A. Di Cicco, L. Bouteillerce and M-H. Li, *Soft Matter*, 2011, **7**, 2613–2623.

8 B. Yan, J. He, P. Ayotte and Y. Zhao, *Macromol. Rapid Commun.*, 2011, **32**, 972–976.

9 A. Peyret, E. Ibarboure, A. Tron, L. Beauté, R. Rust, O. Sandre, N. D. McClenaghan and S. Lecommandoux, *Angew. Chem. Int. Ed.*, 2017, **56**, 1566–1570.

10 S. C. Larnaudie, A. Peyret, L. Beaute, P. Nassoy, S. Lecommandoux, *Langmuir*, 2019, **35**, 8398−8403.

11 K. Chen, G. Xue, G. Shen, J. Cai, G. Zou, Y. Li and Q. Zhang, *RSC Adv.*, 2013, **3**, 8208–8210.

12 W. Su, Y. Luo, Q. Yan, S. Wu, K. Han, Q. Zhang, Y. Gu and Y. Li *Macromol. Rapid Commun.*, 2007, **28**, 1251–1256.

13 E. Mabrouk, D. Cuvelier, F. Brochard-Wyart, P. Nassoy, and M-H. Li, *Proc. Natl. Acad. Sci. U.S.A.*, 2009, **106**, 7294.

14 E. Amstad, S-H. Kim and D. A. Weitz, *Angew. Chem.*, 2012, **124**, 12667–12671.

15 X. Wang, J. Hu, G. Liu, J. Tian, H. Wang, M. Gong, S. Liu, *J. Am. Chem. Soc.*, 2015, **137**, 15262−15275.

16 Y. Sun, F. Gao, Y. Yao, H. Jin, X. Li and S. Lin, *ACS Macro Lett.*, 2021, **10**, 525−530.

17 B. Yan, X. Tong, P. Ayotte and Y. Zhao, *Soft Matter*, 2011, **7**, 10001–10009.

18 A. H. Gelebart, D. J. Mulder, M. Varga, A. Konya, G. Vantomme, E. W. Meijer, R. L. B. Selinger and D. J. Broer, *Nature*, 2017, **546**, 632–636.

19 M. R. Molla, P. Rangadurai, L. Antony, S. Swaminathan, J. J. de Pablo and S. Thayumanavan, *Nat. Chem.*, 2018, **10**, 659–666.

20 G. Wang, X. Tong and Y. Zhao, *Macromolecules*, 2004, **37**, 8911–8917.

21 X. Tong, G. Wang, A. Soldera and Y. Zhao, *J. Phys. Chem. B*, 2005, **109**, 20281–20287.

22 X. Liu and M. Jiang, *Angew. Chem. Int. Ed.*, 2006, **45**, 3846–3850.

23 W. Su, H. Zhao, Z. Wang, Y. Li and Q. Zhang, *Eur. Polym. J.*, 2007, **43**, 657–662.

24 D. Wang, H. Ren, X. Wang and X. Wang, *Macromolecules*, 2008, **41**, 9382–9388.

25 L. Lin, Z. Yan, J. Gu, Y. Zhang, Z. Feng and Y. Yu, *Macromol. Rapid Commun.*, 2009, **30**, 1089–1093.

26 Q. Jin, G. Liu, X. Liu and J. Ji, *Soft Matter*, 2010, **6**, 5589–5595.

27 R. Dong, B. Zhu, Y. Zhou, D. Yan and X. Zhu, *Polym. Chem.*, 2013, **4**, 912–915.

28 Q. Ye, M. Huo, M. Zeng, L. Liu, L. Peng, X. Wang and J. Yuan, *Macromolecules*, 2018, **51**, 3308−3314.

29 L. Li, S. Cui, A. Hu, W. Zhang, Y. Li, N. Zhou, Z. Zhang and X. Zhu, *Chem. Commun.*, 2020, **56**, 6237–6240.

30 L. Li, Y. Li, S. Wang, L. Ye, W. Zhang, N. Zhou, Z. Zhang and X. Zhu, *Polym. Chem.*, 2021, **12**, 3052–3059.

31 Y. Sun, F. Gao, Y. Yao, H. Jin, X. Li and S. Lin, *ACS Macro Lett.*, 2021, **10**, 525−530.

32 W. Wen and A. Chen, *Polym. Chem.*, 2021, **12**, 2447–2456.

33 A. Altomare, F. Ciardelli, B. Gallot, M. Mader, R. Solaro and N. Tirelli, *J. Polym. Sci. A Polym. Chem.*, 2001, **39**, 2957−2977.

34 J. del Barrio, L. Oriol, C. Sanchez, J. L. Serrano, A. Di Cicco, P. Keller and M-H. Li, *J. Am. Chem. Soc.*, 2010, **132**, 3762–3769.

35 E. Blasco, J. L. Serrano, M. Piñol and L. Oriol, *Macromolecules*, 2013, **46**, 5951−5960.

36 G. Cheng and J. Perez-Mercader, *Chem. Mater.*, 2019, **31**, 5691−5698.

37 H. Qian, S. Pramanik and I. Aprahamian, *J. Am. Chem. Soc.*, 2017, **139**, 9140−9143.

38 B. Shao and I. Aprahamian, *Chem.*, 2020, **6**, 2162–2173.

39 X. Guo, B. Shao, S. Zhou, I. Aprahamian and Z. Chen, *Chem. Sci.*, 2020, **11**, 3016–3021.

40 A. Ryabchun, Q. Li, F. Lancia, I. Aprahamian and N. Katsonis, *J. Am. Chem. Soc.*, 2019, **141**, 1196−1200.

41 J. M. Lee, M. B. Koo, S. W. Lee, H. Lee, J. Kwon, Y. H. Shim, S. Y. Kim and K. T. Kim, *Nat. Commun.*, 2020, **11**, 56.

42 M. B. Koo, S. W. Lee, J. M. Lee and K. T. Kim, *J. Am. Chem. Soc.*, 2020, **142**, 14028−14032.

43 M. G. Jeong, J. C. M. van Hest and K. T. Kim, *Chem. Comm.*, 2012, **48**, 3590−3592.

44 Y. La, C. Park, T. J. Shin, S. H. Joo, S. Kang and K. T. Kim, *Nat. Chem.*, 2014, **6**, 534−541.

Chapter 2. Ion-induced macroscopic morphological transformation of poly(ethylene glycol)-*b*-poly(styrene) (PEG-*b*-PS) by modulating the salting-out effect and cation matching effect

2.1 Abstract

The modulation of morphologies of soft nanostructures formed by the solution self-assembly of block copolymers is of significance for a spectrum of applications. In particular, non-synthetic pathways to induce morphological transformation of the block copolymer have been of utmost interest because of the ability to achieve desired morphologies with minimal laborious synthesis. Herein, we report the synthesis of amphiphilic block copolymers composed of tri-arm linear, conventional linear and crown ether end-functionalized hydrophilic polyethylene glycol (PEG) blocks, and hydrophobic polystyrene (PS) blocks. The addition of lithium ions resulted in different extents of salting-out effect in different BCPs due to the architecture and the end-group functionalized hydrophilic segments as the decisive factors. Furthermore, the host-guest recognition between 12-crown-4 ether and lithium cation contributes significantly to the morphological transformation of the polymer vesicles to polymer cubosomes.

2.2 INTRODUCTION

Soft nanostructures, achieved by the self-assembly of block copolymers (BCPs) in solution, have been employed in applications such as drug delivery, nanoreactors, and templates for the synthesis of functional nanostructured materials.[1–9] For their application, it is important to control the size and morphologies of BCP nanostructures by molecular engineering of BCP building blocks. [10–12] A wide range of morphologies, including simple geometric structures (spherical and worm-like micelles), vesicles, and complex bilayer structures, can be accessible from the solution self-assembly of BCPs engineered to possess the defined molecular weights of immiscible polymer segments.[13–16] The structural parameters of BCP building blocks such as molecular weights, block ratios, chemical structures of polymer blocks, and topologies and architectures can be precisely defined by elaborate synthesis of BCPs, which guides the BCP to form nanostructures of desired sizes and shapes. [17–21]

However, this synthetic method of engineering the BCP structures involves tedious multistep synthesis. In addition, the one-to-one correspondence of a BCP to its self-assembled nanostructure complicates the availability of BCP nanostructures for a wide range of applications. Alternative approaches to achieve desired nanostructures without extensive synthetic effort have been intensely pursued. For example, the self-assembly of the BCP blends exhibit a range of morphologies depending on the composition of BCPs having different molecular weights and block ratios.[22–24] Also, the morphology transition of BCP structures has been demonstrated by adjusting the solvent composition used for self-assembly, temperature and addition of ions.[25–31]

In particular, ion-induced morphological transitions of BCP nanostructures have been extensively investigated by Eisenberg and coworkers. They demonstrated that

the presence of salt in water induced morphological variations from the solution self-assembly of a single BCP involving micelles, vesicles, hexagonally packed hollow hoops and large compound micelles (LCMs) and vesicles (LCVs).[31–36] This morphological diversity was achieved by reducing the hydrophilicity of poly(acrylic acid) or poly(ethylene glycol) by the salting-out effect caused by increased salt concentrations. Recently, crown ethers have been introduced to water-soluble polymer systems and demonstrated superior properties as cation extractants in liquid-liquid extraction (LLE) systems and thermodynamic analysis, in particularly, the lower critical solution temperature (LCST) behavior in thermoresponsive systems.[37–42] Crown ethers (CEs) are considered a cyclic version of oligo(ethylene glycol) (OEG) which are attractive due to their ability to chelate selectively to metal cations based on supramolecular host-guest recognition.[43–44] The binding profile of CEs to metal ions in organic solvents distinguishes from that in aqueous environments owing to the fact that intrinsic hydration shell formation and dehydration energy required should be considered.[38] Inspired by the striking effect of CE incorporated polymer systems, we aimed to investigate the possible influence of CE on the classical salting-out effect which can be translated into morphological transformation in our BCP system.

Herein, we report the synthesis of BCPs composed of tri-arm linear, conventional linear and crown ether end-functionalized hydrophilic polyethylene glycol (PEG) blocks, and hydrophobic polystyrene (PS) blocks. We constructed the block ratio of the pristine BCPs to self-assemble into polymersomes. Upon the addition of lithium ions, salting-out effect was maximized in BCP containing tri-arm linear PEG blocks which motivated further exemplary studies involving conventional linear and crown ether end-functionalized PEG blocks. Among the two model BCP systems, the former displayed hydrophilic block architecture as the

dominant factor influencing the extent of salting-out effect determined by the quantity of ions required to induce morphological transformation of the self-assembled structures. However, additional study to trace the morphological transition is necessary which can be proven in the latter system. Notably, the interaction between ethylene segments and water molecules alters to accommodate the ion-water interactions, as well as CE-Li^+ ion-dipole interactions specifically for CE-containing solvophilic blocks. The involvement of noncovalent interactions plays a significant role in the morphological transformation of the self-assembled nanostructures as a function of the salt concentrations (Fig. 2-1). The ubiquitous mechanism underlying the effect of salt additive on morphological transformation of the self-assembled BCPs nanoparticles: salting-out effect is interfered by competitive host-guest complexation which could slow down the rate of morphological transformation toward high-curvature structures. In addition, the lithium guest ions bound to the CE units of the hydrophilic block was confirmed by UV-Vis spectroscopy. The elucidation of our system could allow polymeric morphologies to be tailored via a non-synthetic approach; varying the salt concentrations and stable CE-Li^+ complex to be employed in potential applications.

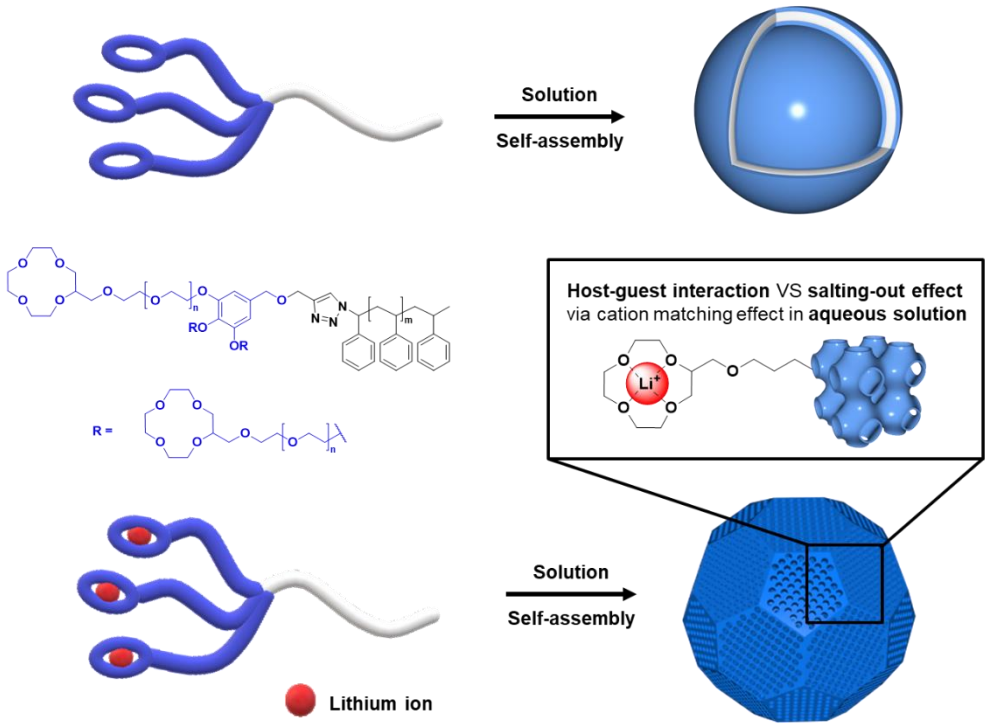

Fig. 2-1 Schematic representation of the LiCl-induced morphological transformation of self-assembled structures of crown ether-functionalized PEG-*b*-PS BCP system.

2.3 RESULTS AND DISCUSSION

Design and synthesis of block copolymers.

To prepare monodisperse hydrophilic blocks, PEGs were synthesized using a previously reported procedure (Scheme 2-2). [47–48] Tetraethylene glycol was orthogonally protected with trityl (Trt) group and tosylate ester (Ts) using trityl chloride in the presence of triethylamine, and 4-toluenesulfonyl chloride, respectively. The resulting heterobifunctional PEG was coupled with tetraethylene glycol and subsequent tosylation to obtain Ts-PEG350-Trt (Fig. 2-8). 12-crown-4 ether was introduced to the end of Ts-PEG350-Trt and reacted with methyl gallate, followed by ester reduction to allow subsequent end-functionalization of alkyne group to generate the crown ether functionalized hydrophilic block (CE-PEG350_3-acetylene) (Scheme 2-2, Fig. 2-9, 2-10, 2-11, 2-12, 2-13 and 2-14). For the polydisperse linear tri-arm (PEG550_3-acetylene) and linear (PEG2000-acetylene) hydrophilic PEG blocks, α-methoxy-ω-tosyl PEGs of the respective molecular weights were installed on methyl gallate, followed by alkyne functionalization. The respective PEG blocks were purified by column chromatography, and their purity was determined by NMR spectroscopy and matrix-assisted laser desorption/ionization time-of-flight (MALDI-TOF) mass spectrometry (Fig. 2-2A, 2-2C, 2-2E, 2-18A, 2-19A and 2-20A).

The corresponding polystyrene (PS) hydrophobic modules (M_n = 6k, 12k, 15k) were synthesized via atom-transfer radical polymerization (ATRP) of the styrene using 1-bromoethylbenzene as an initiator, and subsequent end-group substitution with NaN_3 in DMF to obtain azido terminated polystyrene (PS-N_3) (Scheme 2-3). The synthesis of amphiphilic BCPs composed of PEG hydrophilic blocks coupled to hydrophobic PS blocks via Cu-catalyzed azide-alkyne click chemistry (CuAAC)

was confirmed by ^{1}H NMR spectroscopy and gel permeation chromatography (GPC) (Scheme 2-1, Fig. 2-2B, 2-2D, 2-2F, 2-15, 2-16 and 2-17); the results are summarized in Table 2-1.

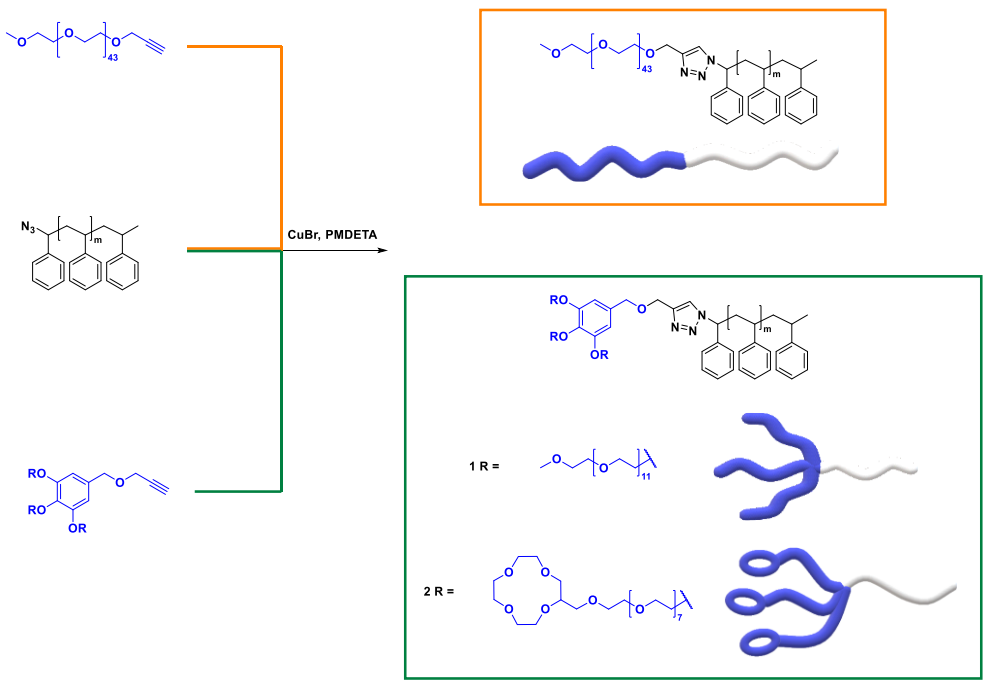

Scheme 2-1 Synthesis of PEG-*b*-PS block copolymers composed of 12-crown-4 ether units and branched linear PEG block (in green box), and linear PEG chain (in orange box) coupled with hydrophobic polystyrene blocks.

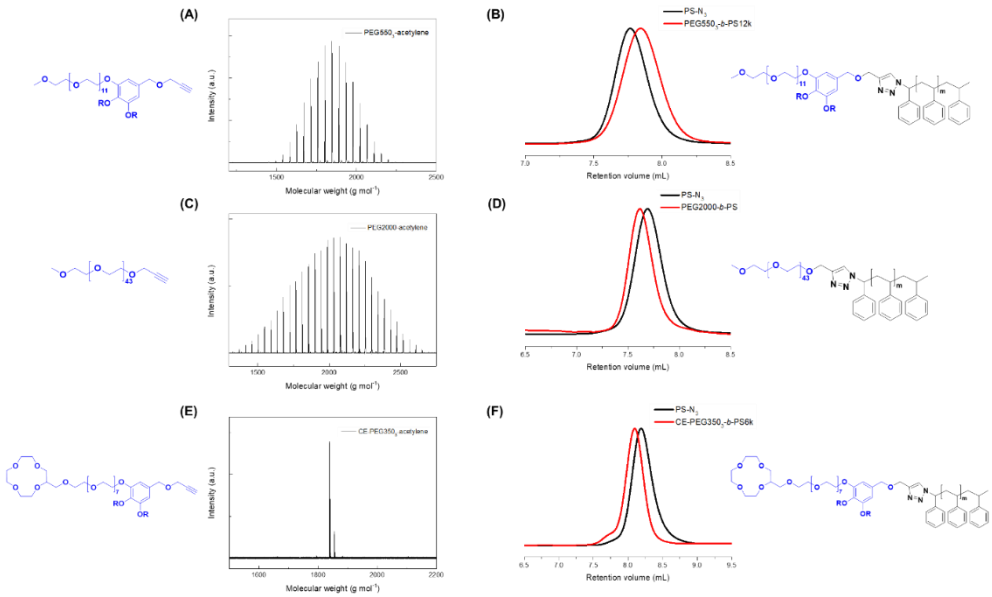

Fig. 2-2 (A, C and E) MALDI-TOF spectra and (B, D and F) GPC (THF) profile of polydisperse PEG550$_3$-acetylene, PEG2000-acetylene, monodisperse CE-PEG350$_3$-acetylene hydrophilic blocks, and their amphiphilic block copolymers respectively.

Table 2-1 Characteristics of amphiphilic block copolymers containing a series of hydrophilic blocks.

Sample	Name	M_n (g/mol)[a] of hydrophilic block	M_n (g/mol)[b] of hydrophobic block	M_n (g/mol)[b] of BCP	$Đ$[b] of BCPs	f_{PEG} (%)[c]
1	$PEG550_3$-*b*-PS12k	1650*	11950	14320	1.06	11.5
2	PEG2000-*b*-PS15k	2000*	15220	17590	1.04	11.4
3	$PEG350_3$-*b*-PS6k	1650	5940	9216	1.06	17.9

[a]Number average molecular weight (M_n) of hydrophilic block was determined by MALDI-TOF spectra. [b]M_n and molecular weight distribution ($Đ$) determined by GPC using polystyrene (PS) standards. Elution was performed with THF at a flow rate of 1 mL min^{-1} at 30 °C. [c]Molecular weight fraction of the PEG domain relative to the amphiphilic block copolymer. *M_n of polydisperse hydrophilic block ($Đ$ > 1).

Concentration of LiCl environment modulates self-assembly behavior and determines the range of accessible morphologies.

Morphological transformation of BCP1 containing branched linear hydrophilic PEG blocks

The BCP composed of polydisperse tri-arm linear hydrophilic PEG block (M_n = 1650 Da, $Đ$ > 1) and hydrophobic PS block ($Đ$ > 1), was allowed to self-assemble

and form nanostructures in water using a co-solvent method. 1,4-dioxane was used as a common solvent to dissolve the BCPs (5 mg/mL). An equal volume of distilled water was slowly added at a rate of 0.5 mL/h using a syringe pump to the solvent to induce self-assembly of the BCP. The dialysis of medium was performed against water for 24 h. The morphologies of the aggregates in the aqueous suspension were observed with scanning electron microscopy (SEM) and transmission electron microscopy (TEM). The analyses results revealed that **BCP1** ($PEG550_3$-*b*-PS12k) self-assembled into spherical polymersomes in water (Fig. 2-3A, 2-3B and 2-5). To induce morphological transitions of the BCP, increasing concentrations of LiCl solution were added to self-assemble the BCP. Upon the addition of 0.1 M LiCl solution, the polymersomes of **BCP1** transformed into cubosomes directly without intermediate morphologies (Fig. 2-3C, 2-3D, 2-21A and 2-21B). The generation of cubosomes extends to 0.4 M of LiCl solution, which subsequently resulted in particle aggregation with further increase in the concentration of LiCl (Fig. 2-3E, 2-3F, 2-3G, 2-3H, 2-3I, 2-3J, 2-21 and 2-22).

We attributed the rapid morphological transformation of **BCP1** to salting-out effect as the decisive factor. In a typical salting-out effect, upon salt addition, the added ions accumulate around the PEG segments which leads to the contraction and subsequent decrease in the steric interchain repulsion between the hydrophilic PEG blocks, causing the expansion of the core till the point where morphological transformation occur to reduce the entropic penalty due to the PS chain stretching.[35] The low density of the linear branched PEG chains in **BCP1** due to the short PEG chains can cause loss of colloidal stability which further subjects the colloid to higher sensitivity towards the salt, and induced morphological transformations within low salt concentrations (Fig. 2-6A).[45]

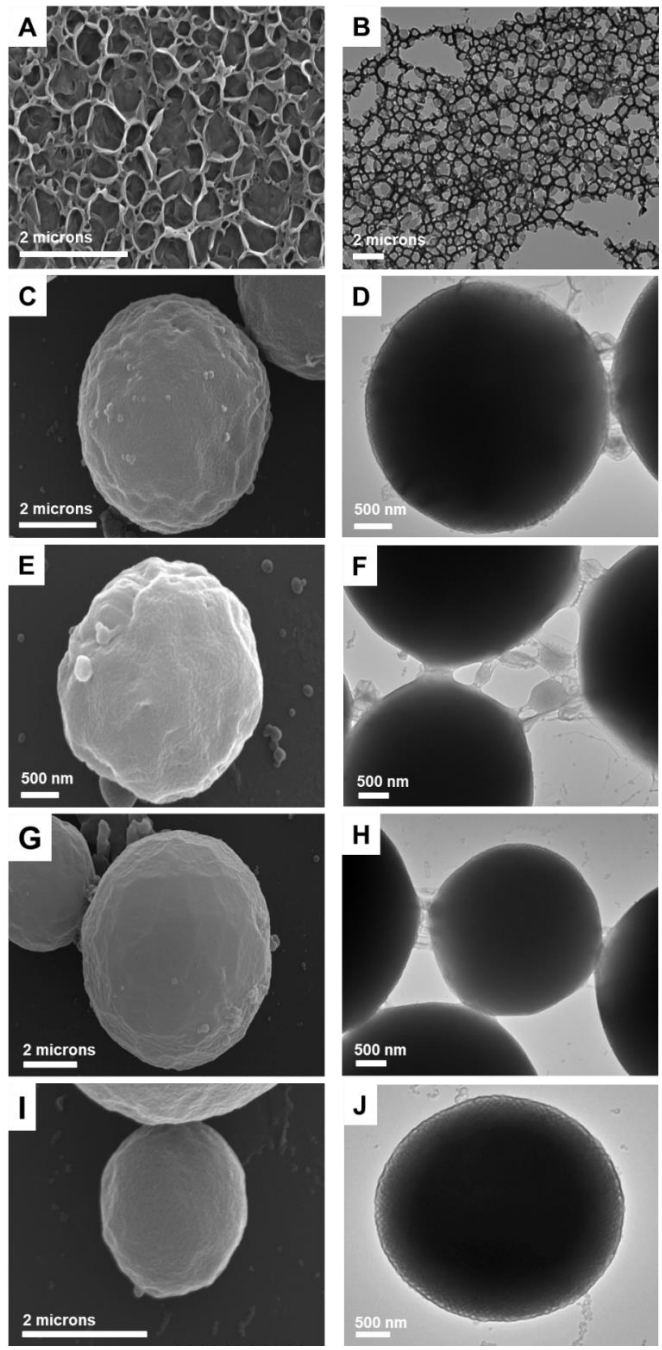

Fig. 2-3 SEM and TEM images of self-assembled structures of PEG550$_3$-*b*-PS12k under (A and B) 0 M, (C and D) 0.1 M, (E and F) 0.2 M, (G and H) 0.3 M, and (I and J) 0.4 M of LiCl respectively.

1) Effect of the architecture of hydrophilic block in the BCP backbone

The salting-out effect was maximized in the **BCP1** system which posed a difficulty to control the salt concentration for the study of morphological transformation. Therefore, to gain deeper insight of the salting-out effect translated in the morphological transformation of the self-assembled structures, we introduced conventional linear PEG block (M_n = 2000 Da, $Đ$ > 1) and synthesized **BCP2**. When self-assembled by the same co-solvent method as that used in the case of **BCP1**, **BCP2** (PEG2000-*b*-PS15k) self-assembled into spherical polymersomes in water (Fig. 2-4A and 2-5). The polymersomes of **BCP2**, did not undergo morphological transformation until self-assembly under 1.5 M of LiCl where the polymersomes were present along with a mixture of spongesomes and cubosomes (Fig. 2-4B, 2-4C, 2-5, 2-23A and 2-23B). As the concentration increases to 2.0 M, the population of cubosomes and hexosomes dominates in the mixture containing vesicles and lamella (Fig. 2-4D, 2-23C and 2-23D). Further increase in the concentration beyond 2.1 M resulted in intermediate precipitation (Fig. 2-4E and 2-5). To explain this phenomenon, we suggest that the long linear PEG block implies the high surface densities of the corona chain would be expanded from the core due to the strong interchain repulsion, which resulted in a weakened salting-out effect observed in the delayed morphological transformation (Fig. 2-6B).[46]

2) Effect of the end-group functionalized hydrophilic block in the BCP backbone

We found that **BCP2** polymersomes require relatively higher concentrations of LiCl to induce morphological transformation of the self-assembled nanostructures compared to that of **BCP1**. The architecture of hydrophilic PEG block influences the salting-out effect on the BCP nanoparticles, however, notably, only a mixture of metastable particles was existent throughout the self-assembly process across the entire range of LiCl concentration in **BCP2**. Encouraged by the findings of **BCP1**, we hypothesized that other factors besides PEG block architecture, might also contribute to a different morphological trend. Therefore, we synthesized **BCP3** comprising discrete crown ether functionalized tri-arm hydrophilic PEG block having the same molecular weight (M_n = 1650 Da, $Đ$ = 1) as that of **BCP1**. The prepared **BCP3** (CE-PEG350$_3$-*b*-PS6k) self-assembled into spherical vesicles (Fig. 2-4F, 2-5 and 2-24A). Increasing LiCl concentrations were added during the self-assembly process to induce morphological transitions of **BCP3**. The addition of 0.2 M LiCl solution caused the polymersomes of **BCP3** to increase in size along with the emergence of a minor population of lamella (Fig. 2-24B). As the concentration of LiCl solution increased from 0.4 M to 1.2 M, the mixture of polymersomes and lamella density fluctuations and transformed gradually to a significant increase in spongesomes among the existing population (Fig. 2-4G, 2-24C, 2-24D, 2-24E and 2-24F). The disappearance of the polymersomes was confirmed when **BCP3** was self-assembled under 1.4 M to 1.6 M LiCl solution, favoring the formation of cubosomes (Fig. 2-4H, 2-24G, 2-24H and 2-26A). Subsequently, the addition of 1.7 M to 2.0 M LiCl solution led to spongesomes coexisting with cubosomes as the dominant morphologies (Fig 2-4I, 2-25A, 2-25B, 2-26B and 2-26C). Finally at 2.2 M LiCl solution, **BCP3** self-assembled into exclusively cubosomes (Fig. 2-4J, 2-

25C, 2-25D and 2-26D). It is noted that further increasing the concentration of LiCl beyond 2.2 M led to aggregation.

We attributed the slow morphological transformation of **BCP3** to the competitive host-guest interaction between the crown-ether moieties and lithium ions, and salting-out effect (Fig. 2-6C). In terms of the architecture of the PEG block, the presence of cyclic PEG in **BCP3** increases the overall density of the PEG chains due to the intrinsic smaller hydrodynamic volume despite having the same PEG molecular weight in **BCP1**. The architecture could have contributed to the morphological trend to a certain extent, however the decisive factor is more likely due to the complexation between the oxygen atoms and lithium ions, introducing ion-dipole interactions. [38] The host-guest binding contributes to a salting-in effect which establishes an equilibrium with the salting-out effect, depending on the concentration of salt added. [40] High amount of energy is required to overcome the strong hydration shell of lithium however depending on the concentration of the added salt, salting-in effect dominates over salting-out effect when the equilibrium favors. [40] The electrostatic interactions interfere with the salting-out effect, resulting in a slow morphological transformation for **BCP3**.

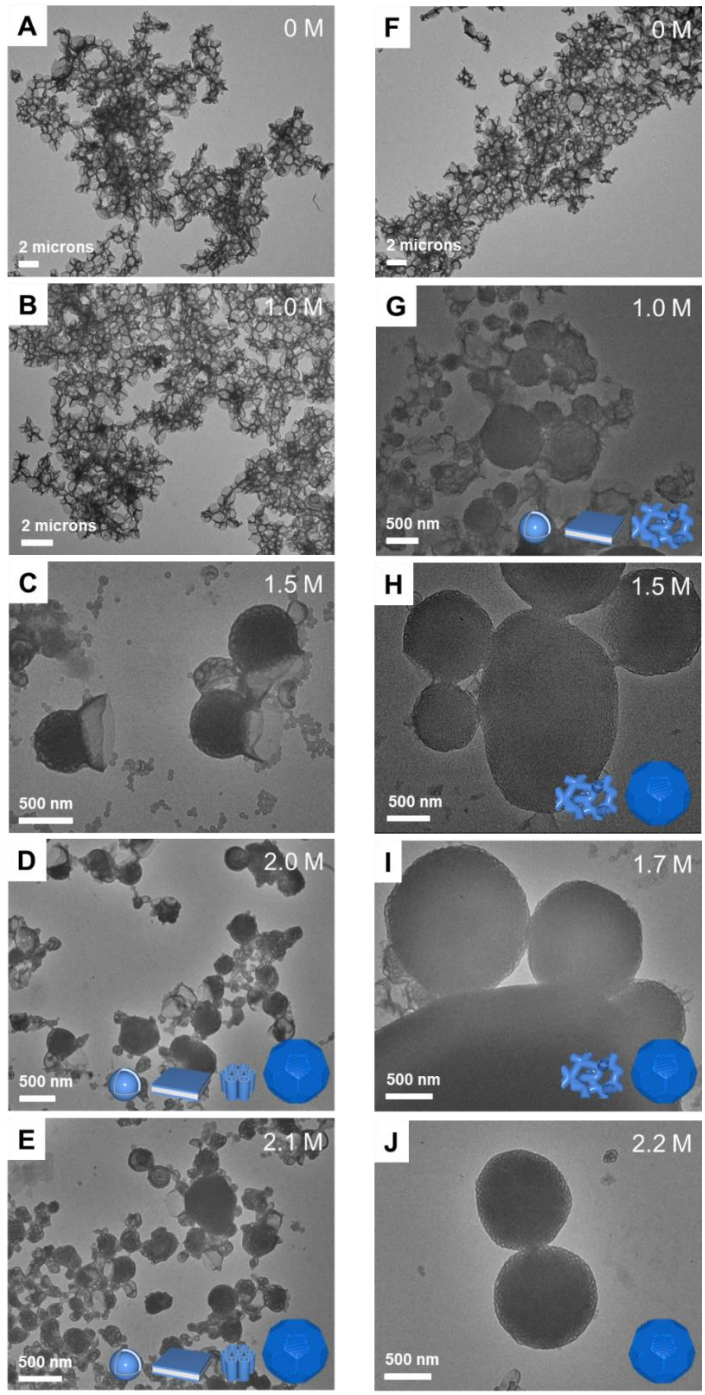

Fig. 2-4 TEM images of self-assembled structures of (A to E) PEG2000-*b*-PS15k and (F to J) CE-PEG350$_3$-*b*-PS6k under different concentrations of LiCl.

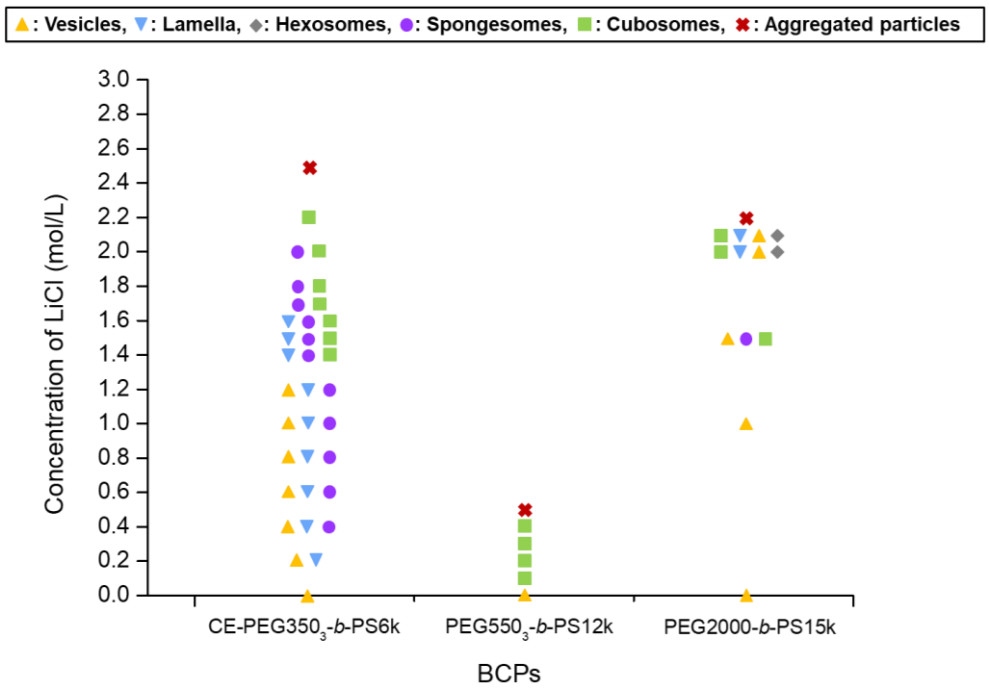

Fig. 2-5 Morphological phase diagram of the respective self-assembled BCPs as a function of LiCl concentration.

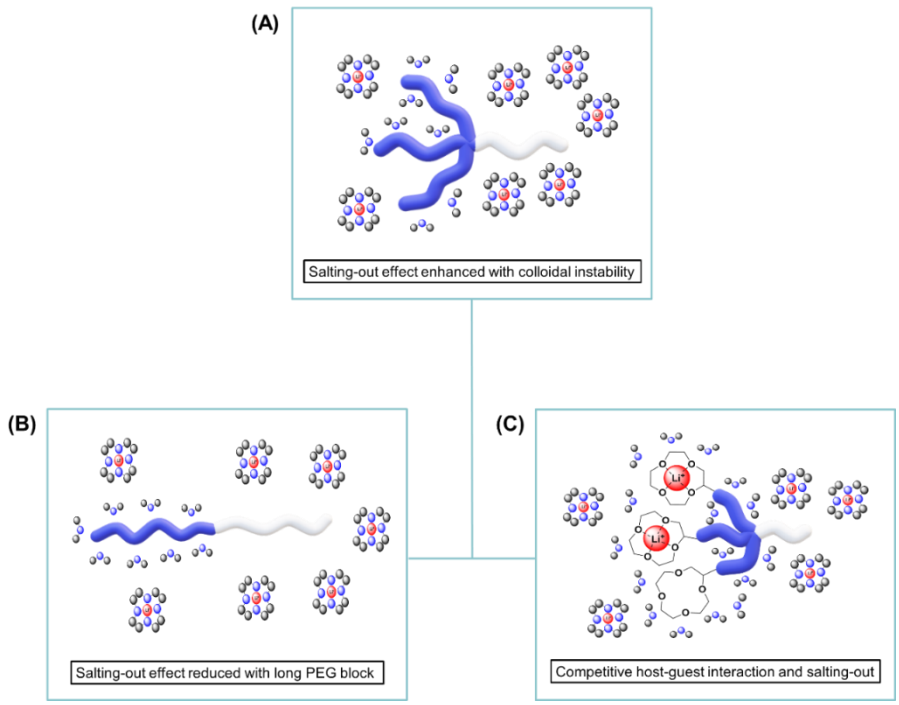

Fig. 2-6 Schematic illustration of the possible mechanisms for the morphological transition of the BCPs (A) PEG550$_3$-*b*-PS12k, (B) PEG2000-*b*-PS15k, and (C) CE-PEG350$_3$-*b*-PS6k after solution self-assembly with LiCl respectively.

Host-guest recognition during solution self-assembly of BCPs in lithium 3,5-diiodosalicylate (LIS)

To prepare the self-assembled nanostructures with similar diameter sizes, appropriate concentrations of LIS dissolved in water was added using a syringe pump to the dioxane solution containing the respective BCPs. The dialysis of medium was performed against water for 24 h. The average size of the aggregates in the aqueous suspension for the three BCPs were confirmed with dynamic light

scattering (DLS) and were revealed to be approximately 500 nm (Fig. 2-7A). The UV-Vis spectroscopic analysis of LIS; a UV responsive lithium salt in water revealed the absorption maximum (λ_{max}) at 323 nm (Fig. 2-7B).[38] To investigate the lithium complexation ability of the respective BCPs in water, 0.05 M , 0.5 M and 0.5 M of LIS were added to the dioxane solution of **BCP1**, **BCP2** and **BCP3** respectively. The UV-Vis analysis of **BCP3** (CE-PEG350$_3$-*b*-PS6k) revealed two signals corresponding to the λ_{max} of LIS and polystyrene at around 280 nm which constitutes the hydrophobic block in the BCP (Fig. 2-7B).[38] The presence of LIS in the UV-Vis analysis proves host-guest interaction between **BCP3** functionalized with 12-crown-4 ether and lithium ion was spontaneous to a certain extent in aqueous solution. The monotonic function is attributed to the presence of self-assembled solid nanoparticles which caused light scattering during the UV-Vis analysis. In contrast, **BCP1** and **BCP2** showed absence of the peak corresponding to the LIS which proves poor retainment of the lithium ion in aqueous solutions.

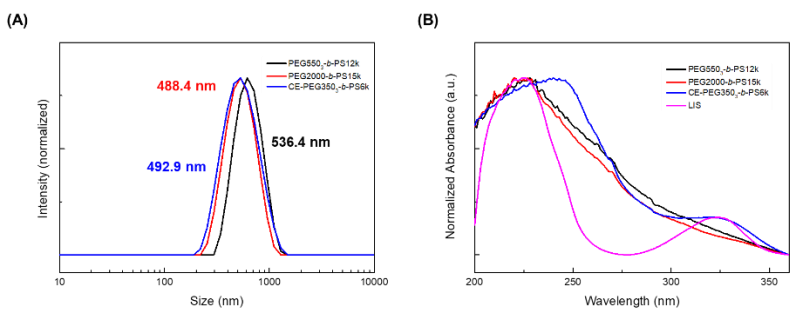

Fig. 2-7 (A) DLS size plots and (B) UV-Vis spectra of the amphiphilic block copolymers after solution self-assembly with the LIS salt respectively.

2.4 CONCLUSION

In summary, we synthesized BCPs composed of hydrophilic PEG blocks: tri-arm linear, conventional linear and branched crown ether end-functionalized, and hydrophobic PS blocks of varying molecular weights. The BCPs self-assembled into nanostructures via a cosolvent self-assembly method. We found that the macroscopic morphological transformation of the self-assembled nanoparticles can be achieved upon the creation of an ionic environment during solution self-assembly. The self-assembled nanostructures of BCP with branched linear PEG chain undergo expeditious morphological transformation without immediate morphologies. In contrast, the nanoparticles constructed with BCPs containing linear PEG chain revealed slow delayed morphological transformation which indicates the architecture of the PEG blocks affect the extent of salting-out which resulted in a distinct effect on morphological transformation of the nanoparticles driven by salt-induced environment. Furthermore, the BCP system containing branched crown ether units embedded in the peripheral chains as a dendritic scaffold exhibited gradual morphological transformation. This phenomenon highlighted that the end-group functionalization of hydrophilic block determines the presence of interplay between host-guest recognition and salting-out effect. The precise modulation of morphologies in our system can contribute significantly to the design and development of BCPs for the fabrication of polymer cubosomes in aqueous systems, circumventing the need for post functionalization to allow more facile generation of surface functionalized polymer cubosomes for a diverse range of potential applications.

2.5 Experimental Section

1. Materials and methods

General

Unless otherwise noted, all reagents and chemicals were purchased from Sigma Aldrich, Alfa Aesar and TCI and used as received. Styrene was purified prior to polymerization over aluminum oxide. Dichloromethane (CH_2Cl_2) was distilled over CaH_2 under N_2. Tetrahydrofuran (THF) was refluxed over a mixture of Na and benzophenone under N_2 atmosphere and distilled before use. All reactions were performed under an inert atmosphere unless otherwise stated.

Methods

^{1}H and ^{13}C NMR spectra were recorded on Agilent 500-MR DD2 Magnetic Resonance System and Varian/Oxford AS-500 using CD_2Cl_2 and $CDCl_3$ as solvents and internal standards. Molecular weights and dispersity D of polymers and block copolymers were measured by Agilent 1260 Infinity gel permeation chromatography (GPC) system equipped with a PL gel 5 μm MiniMIX-D column (Agilent Technologies) and differential refractive index detectors. THF was used as an eluent with a flow rate of 1 mL min^{-1} at 30 °C. A PS standard kit (Agilent Technologies) was used for calibration. Matrix-assisted laser desorption/ionization time-of-flight mass spectrometry (MALDI-TOF-MS) was performed on Bruker Ultraflex II TOF/TOF mass spectrometer equipped with a nitrogen laser (335 nm). The analytical sample was prepared by mixing a THF solution of an analyte with a THF solution of 2-(4-Hydroxyphenylazo)benzoic acid (HABA) matrix. Conventional TEM was performed on a Hitachi 7600 operating at 100 kV. Specimens were prepared by placing a drop of the sample solution on a carbon-

coated Cu grid (200 mesh, EM science) and then air-drying the grid overnight. Scanning electron microscopy (SEM) was performed on Hitachi S-4300 operating at 15kV. The suspension was cast and dried on a slide glass and coated with Pt using a Hitachi E-1030 ion sputter. Dynamic light scattering (DLS) was performed on Malvern Zetasizer Nano-S. The dialyzed self-assembled polymer solution was diluted with water and an aliquot of 4 mL of the diluted solution was transferred into a plastic cuvette for measurement. Intensity data from each sample were collected in three replicates at 25 °C. UV-Vis spectrometry was measured on a Shimadzu UV-2600i spectrophotometer with a range of 200–600 nm. The dialyzed self-assembled polymer solution was diluted with water and transferred into a plastic cuvette for measurement. All samples were measured in water.

2. Preparation of crown-ether functionalized hydrophilic block

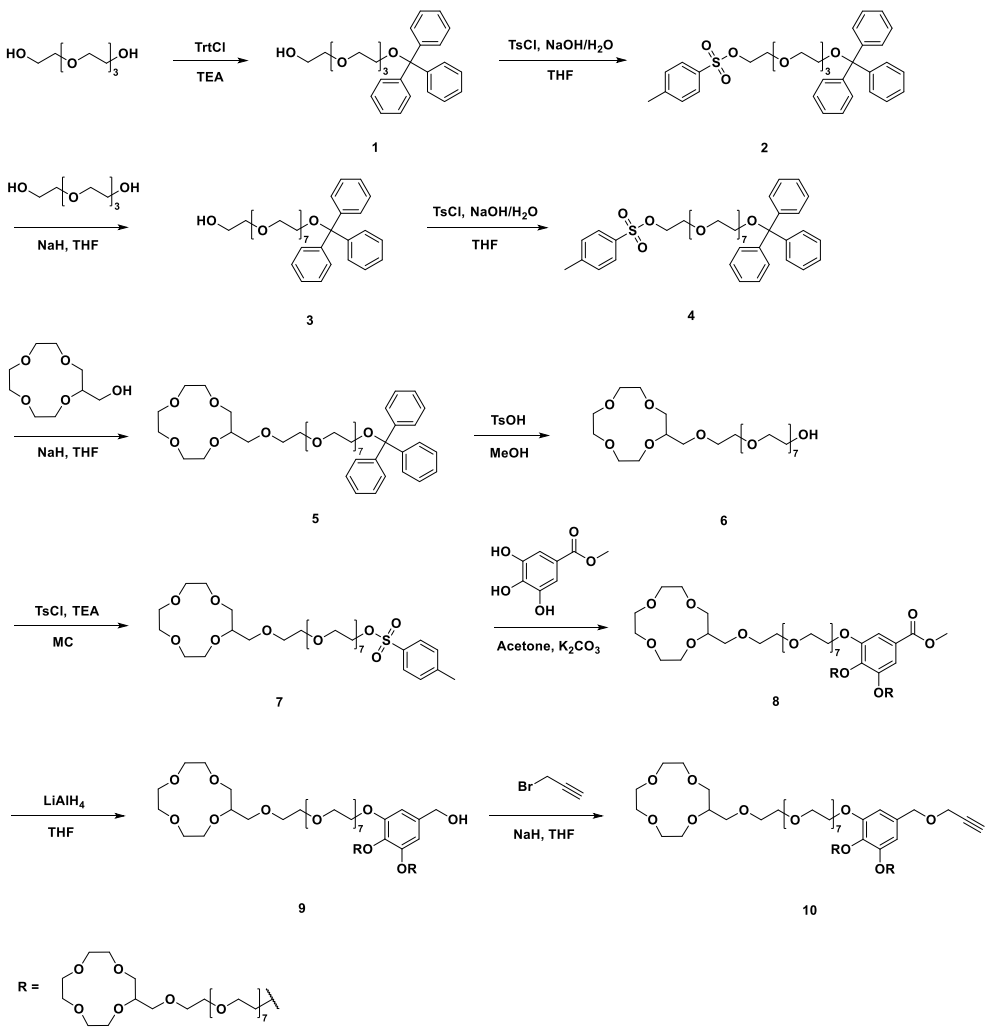

Scheme 2-2 Synthesis of 12-crown 4-ether functionalized PEG chain.

Ts-PEG350-Trt (4). It is synthesized in multi-gram quantity by following the literature methods. [47,48]

^{1}H NMR (500MHz, $CDCl_3$): 7.78 (d, 2H), 7.44 (d, 6H), 7.36–7.18 (m, 11H), 4.11 (t, 2H), 3.72–3.54 (m, 28H), 3.21 (t, 2H), 2.42 (s, 3H) ppm.

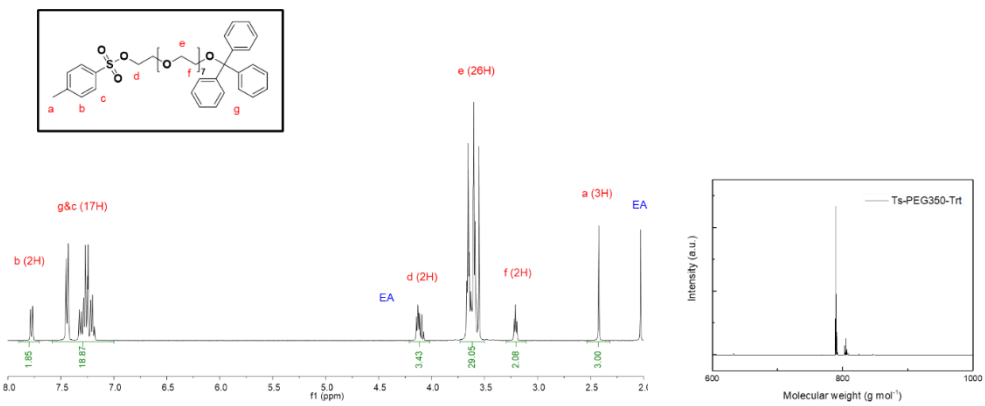

Fig. 2-8 ^{1}H NMR spectra of Ts-PEG350-Trt.

CE-PEG350-Trt (5). A schlenk flask was purged with N_2 and charged with 2-hydroxymethyl-12-crown-4 ether and freshly distilled THF at 0 ^{o}C. To the solution, NaH was added and then the mixture was stirred for 1 h. The Ts-PEG350-Trt (4) in THF was added into the solution. The reaction was stirred at room temperature overnight. The mixture was poured into water and extracted with MC and combine the organic layers. The mixture was washed with saturated solution of ammonium chloride and brine. The organic phase was dried over Na_2SO_4. After removing the solvent, the crude product was purified by flash column chromatography to afford the pure product as colorless liquid.

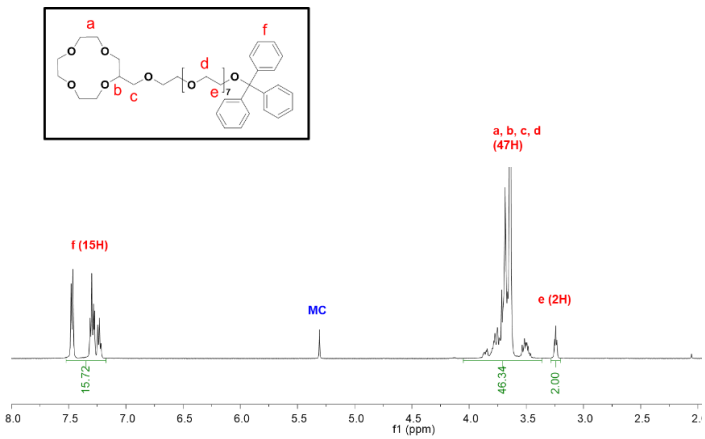

Fig. 2-9 ^{1}H NMR spectra of CE-PEG350-Trt.

CE-PEG350-OH (6). Toluenesulfonic acid monohydrate was added to the solution of CE-PEG350-Trt (5) in MeOH. The reaction mixture was stirred at room temperature for 3 h. Sodium bicarbonate was added to quench the reaction and concentrated under vacuum. The mixture was then redissolved and filtered under gravity filtration followed by washing with MC and brine. The organic layer was collected and dried over anhydrous $MgSO_4$. After removing the solvent, the crude product was purified by flash column chromatography affording a colorless liquid.

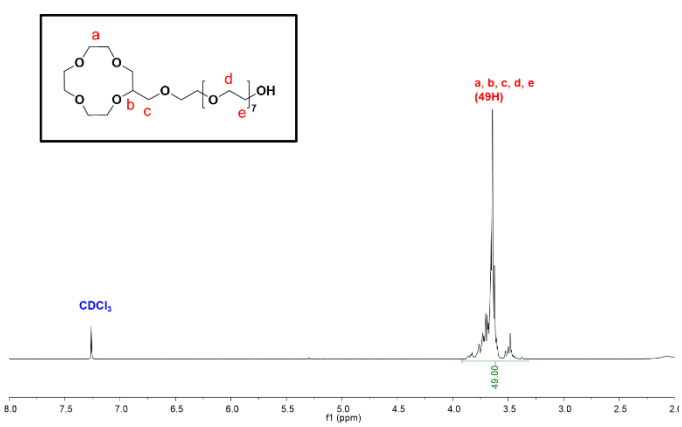

Fig. 2-10 ^{1}H NMR spectra of CE-PEG350-OH.

CE-PEG350-Ts (7). A schlenk flask was purged with N_2 and charged with CE-PEG350-OH (6) and freshly distilled MC. To the solution, TEA was added and then the mixture was stirred for 1 h. Tosyl chloride was added into the solution at 0 °C. The reaction mixture was stirred at room temperature overnight. The mixture was poured into water and extracted with MC and combine the organic layers. The mixture was washed with brine and dried over anhydrous $MgSO_4$. After removing the solvent under reduced pressure, the crude product was purified by flash column chromatography to afford a colorless viscous oil.

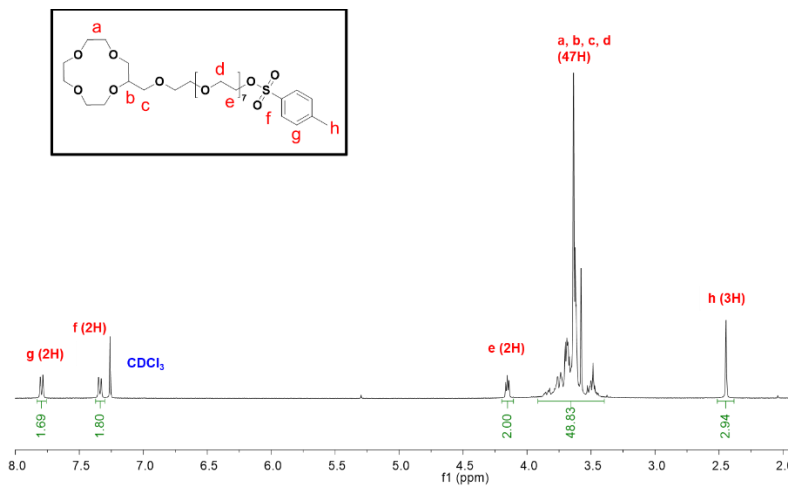

Fig. 2-11 ^{1}H NMR spectra of CE-PEG350-Ts.

CE-PEG350$_3$-benzoate (8). K_2CO_3 was added to a solution of methyl 3,4,5-trihydroxybenzoate and CE-PEG350-Ts (7) in acetone. The reaction was refluxed at 70 °C overnight. After removal of the solvent under vacuum, water was added and the mixture was extracted with MC. The organic phase was dried over $MgSO_4$ and filtered. The solvent was removed by rotary evaporation and then purified by flash column chromatography affording the product.

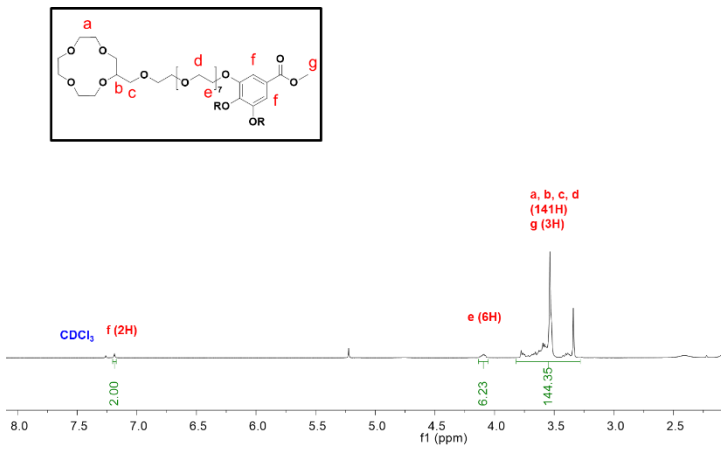

Fig. 2-12 ^{1}H NMR spectra of CE-PEG350$_3$-benzoate.

CE-PEG350$_3$-OH (9). $LiAlH_4$ was added to a solution of CE-PEG350$_3$-benzoate (8) in distilled THF at 0 ºC. The reaction was stirred at room temperature for 3 h. Upon completion of the reaction, the reaction was quenched with 1M HCl followed by dilution with water. The organic layer was separated and washed with brine. The combined organic layer was dried over $MgSO_4$, and the solvent was removed under reduced pressure. The crude product was purified by column chromatography affording a pale yellow viscous oil.

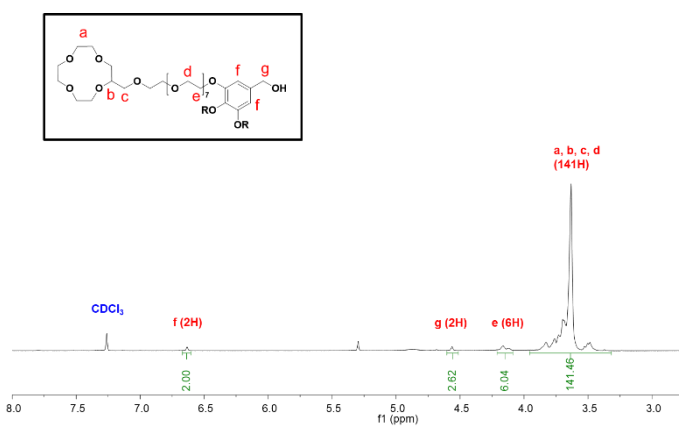

Fig. 2-13 ^{1}H NMR spectra of CE-PEG350$_3$-OH.

CE-PEG350$_3$-acetylene (10). CE-PEG350$_3$-OH (9) was dissolved in dry THF and the mixture was cooled to 0 ^{o}C on an ice bath. To the mixture, NaH was added and stirred for 1 h. Propargyl bromide was then added to the solution and stirred overnight at room temperature. Saturated solution of ammonium chloride was added to quench the reaction and concentrated under reduced pressure. The organic layer was separated and washed with brine. The combined organic layer was dried over $MgSO_4$, and the solvent was removed under vacuum. The crude product was purified by column chromatography affording a pale yellow viscous oil.

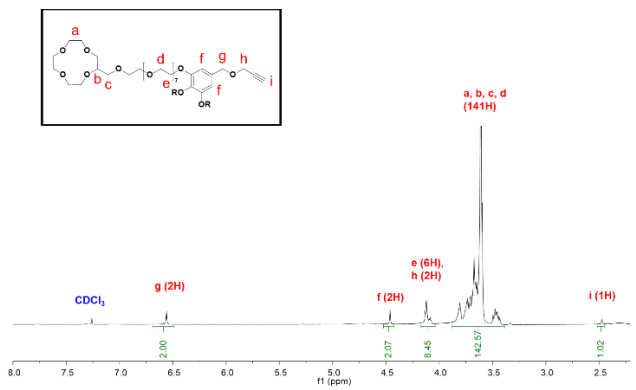

Fig. 2-14 ^{1}H NMR spectra of CE-PEG350$_3$-acetylene.

3. Synthesis of hydrophobic azide-functionalized polystyrene

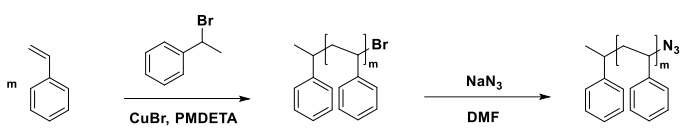

Scheme 2-3 Synthesis of azide-functionalized PS block.

PS-N$_3$. It is synthesized in multi-gram quantity by following the literature methods.[49,50,51]

4. Synthesis of polyethylene glycol-*b*-polystyrene block copolymers

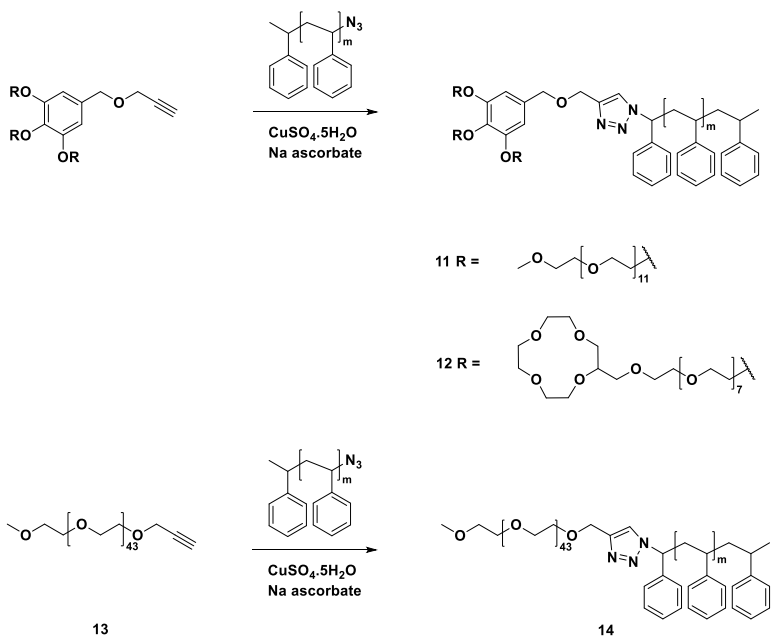

Scheme 2-4 Synthesis of block copolymers having linear branched ($PEG550_3$-*b*-PS12k), 12-crown-4 ether branched (CE-$PEG350_3$-*b*-PS6k) and linear PEG (PEG2000-*b*-PS15k) chains.

$PEG550_3$-*b*-PS12k, PEG2000-*b*-PS15k, CE-$PEG350_3$-*b*-PS6k (11, 14, 12). The respective acetylene-functionalized hydrophilic blocks, azido end-functionalized polystyrene, $CuSO_4.5H_2O$ and sodium ascorbate were dissolved in DMF under N_2 atmosphere. The mixture was purged with N_2 for 15 min and stirred overnight at room temperature. The CuAAC reaction was monitored by GPC and after the consumption of hydrophilic block, the solvent is removed under vacuum. The

crude product was purified by column chromatography to afford the pure product as white solid.

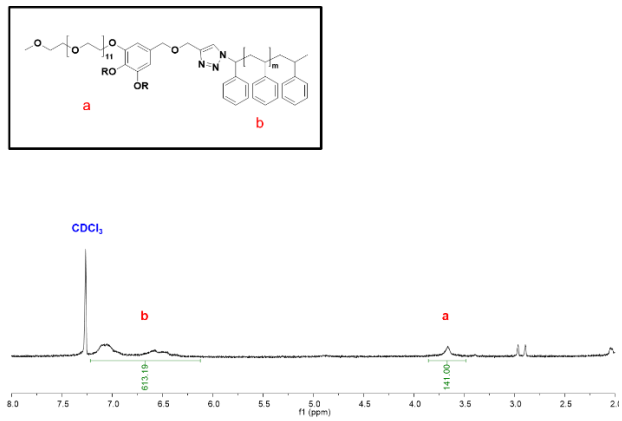

Fig. 2-15 ^{1}H NMR spectra of PEG550$_3$-*b*-PS12k.

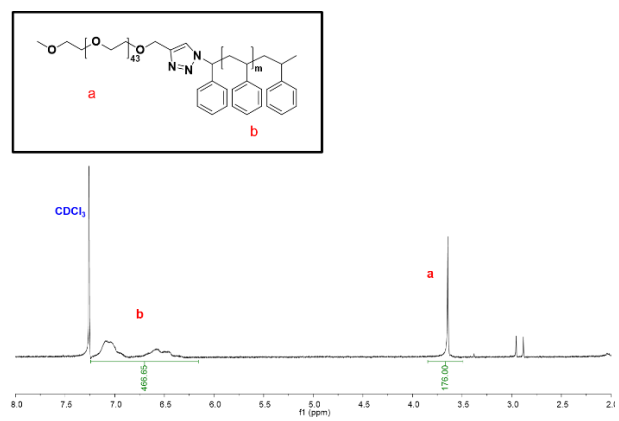

Fig. 2-16 ^{1}H NMR spectra of PEG2000-*b*-PS15k.

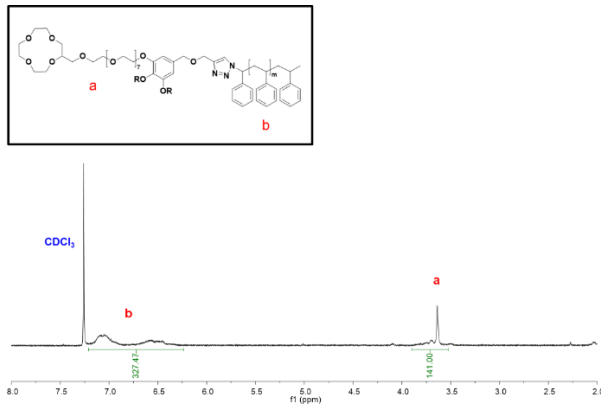

Fig. 2-17 ^{1}H NMR spectra of CE-PEG350$_3$-*b*-PS6k.

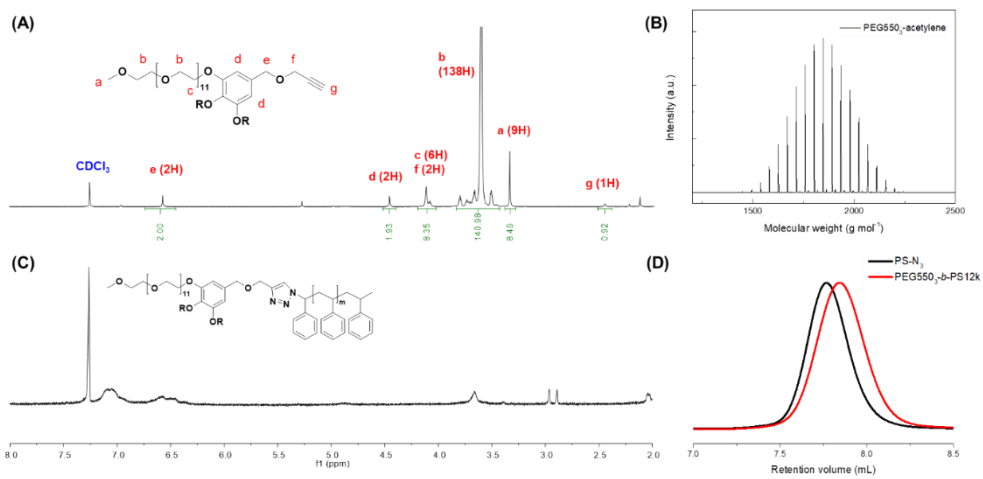

Fig. 2-18 (A and C) ^{1}H NMR spectra in $CDCl_3$ and (B and D) MALDI-TOF spectra and GPC (THF) profile of polydisperse hydrophilic block (PEG550$_3$-acetylene) and amphiphilic block copolymer (PEG550$_3$-*b*-PS12k) respectively.

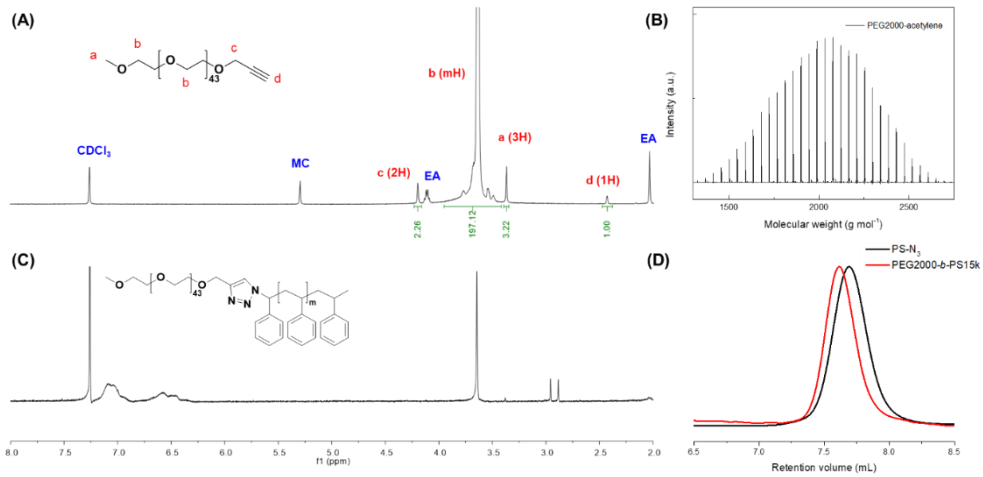

Fig. 2-19 (A and C) ^{1}H NMR spectra in $CDCl_3$ and (B and D) MALDI-TOF spectra and GPC (THF) profile of polydisperse hydrophilic block (PEG2000-acetylene) and amphiphilic block copolymer (PEG2000-*b*-PS15k) respectively.

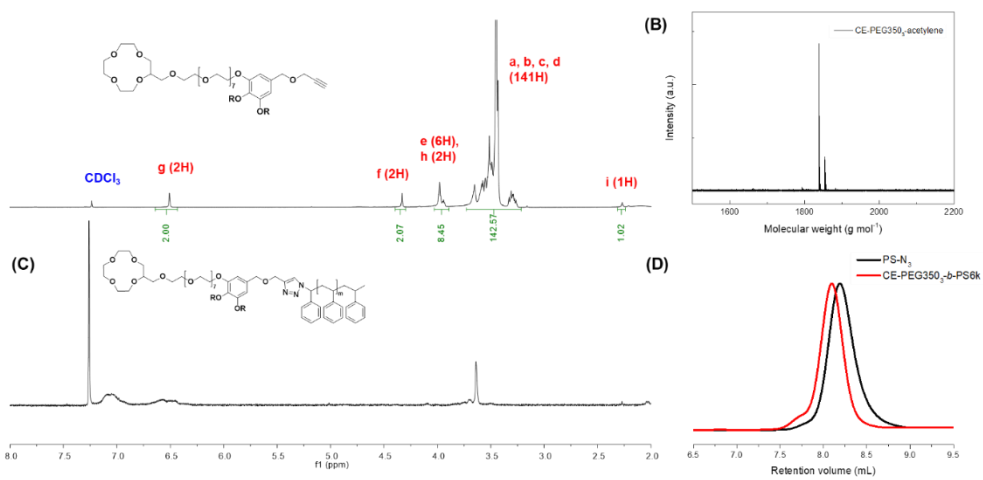

Fig. 2-20 (A and C) ^{1}H NMR spectra in $CDCl_3$ and (B and D) MALDI-TOF spectra and GPC (THF) profile of monodisperse hydrophilic block (CE-PEG350$_3$-acetylene) and amphiphilic block copolymer (CE-PEG350$_3$-*b*-PS6k) respectively.

5. Solution self-assemblies of BCPs via co-solvent method

5 mg of BCPs was dissolved in dioxane (1 mL) in a 20 mL capped vial with magnetic stirrer. The solution was stirred for 1 h at room temperature (860 rpm). A syringe pump was calibrated to inject water at a speed of 0.5 mL/h. The vial cap was replaced with a rubber septum, and water was added to the polymer solution over 2 h using a syringe pump with a 6-mL syringe equipped with a steel needle. However, different concentrations of lithium chloride were dissolved in water and added to the polymer solution over 2 h for the self-assembly in salt environment. The resulting suspension was subjected to dialysis (molecular weight cutoff 12-14 kDa (SpectraPor, Rancho Dominguez, CA)) against water for 24 h.

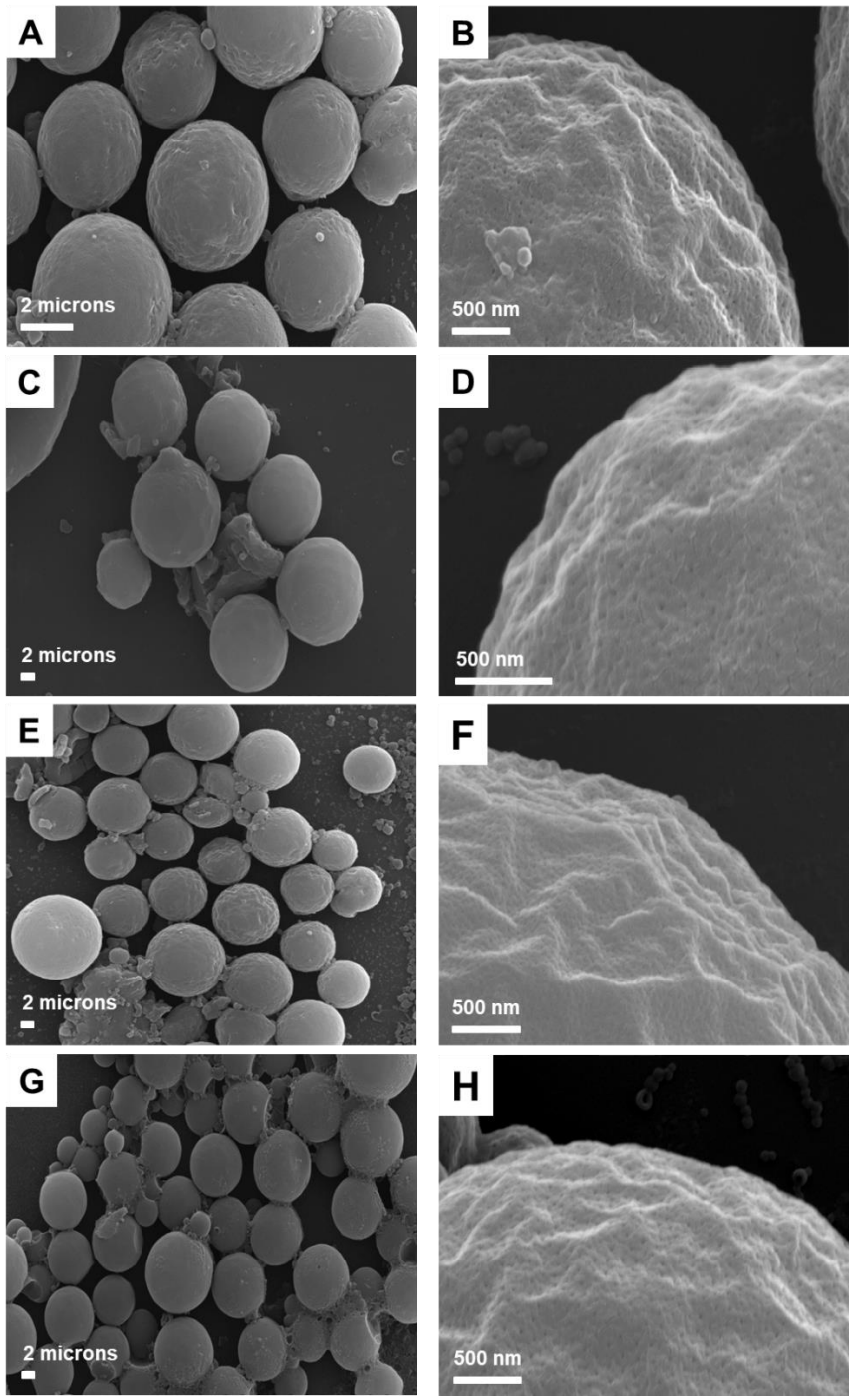

Fig. 2-21 SEM images of self-assembled structures of PEG550$_3$-*b*-PS12k under (A and B) 0.1 M, (C and D) 0.2 M, (E and F) 0.3 M, and (G and H) 0.4 M of LiCl.

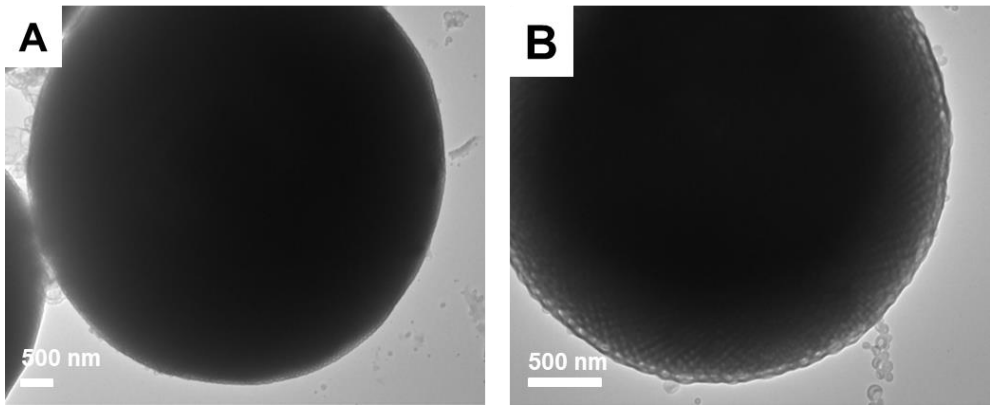

Fig. 2-22 TEM images of polymer cubosomes of PEG550$_3$-*b*-PS12k under 0.4 M of LiCl.

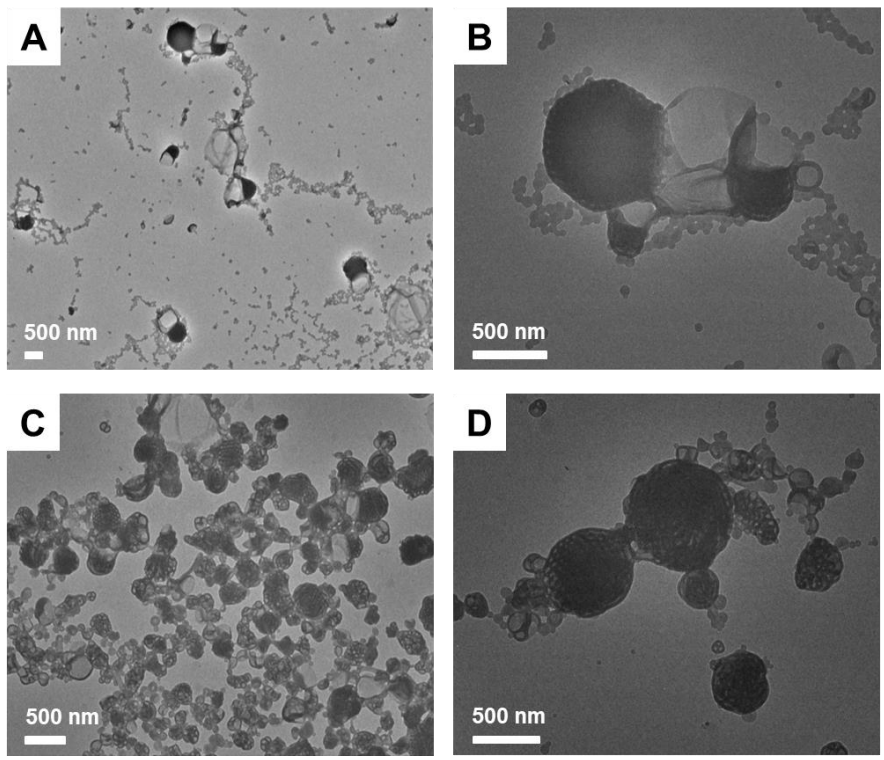

Fig. 2-23 TEM images of self-assembled structures of PEG2000-*b*-PS15k under (A and B) 1.5 M, and (C and D) 2.0 M of LiCl.

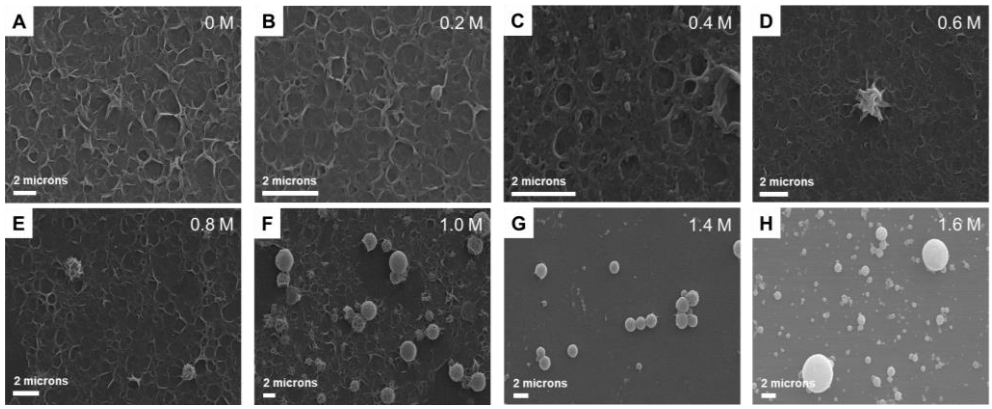

Fig. 2-24 SEM images of self-assembled structures of CE-PEG350$_3$-*b*-PS6k under different concentrations of LiCl ranging from 0 M to 1.6 M.

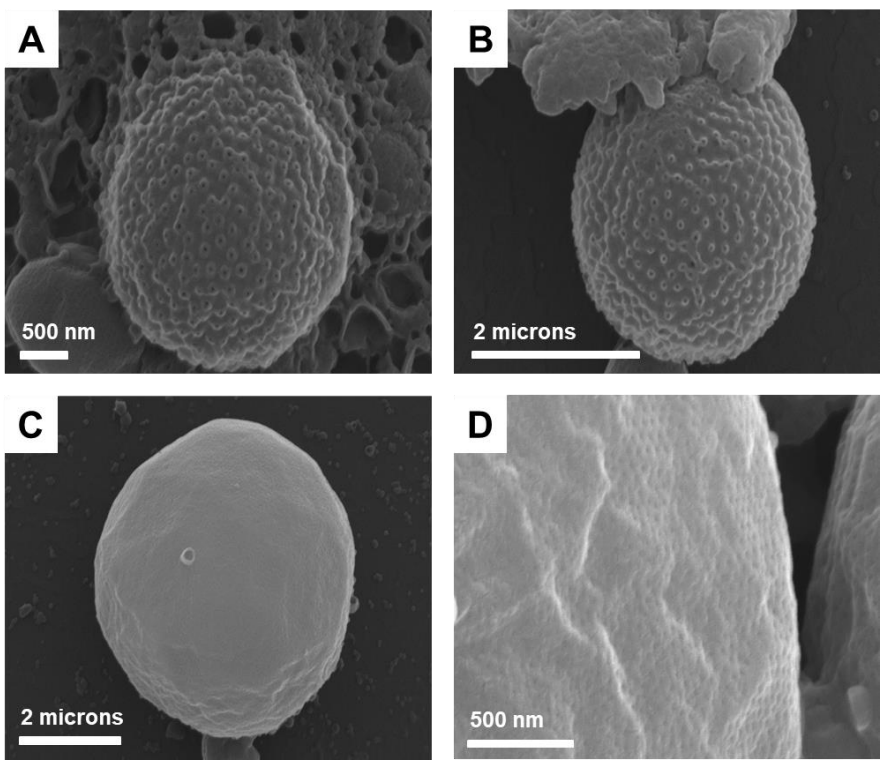

Fig. 2-25 SEM images (A and B) spongesomes, and (C and D) cubosomes of CE-PEG350$_3$-*b*-PS6k under 1.7 M and 2.2 M of LiCl respectively.

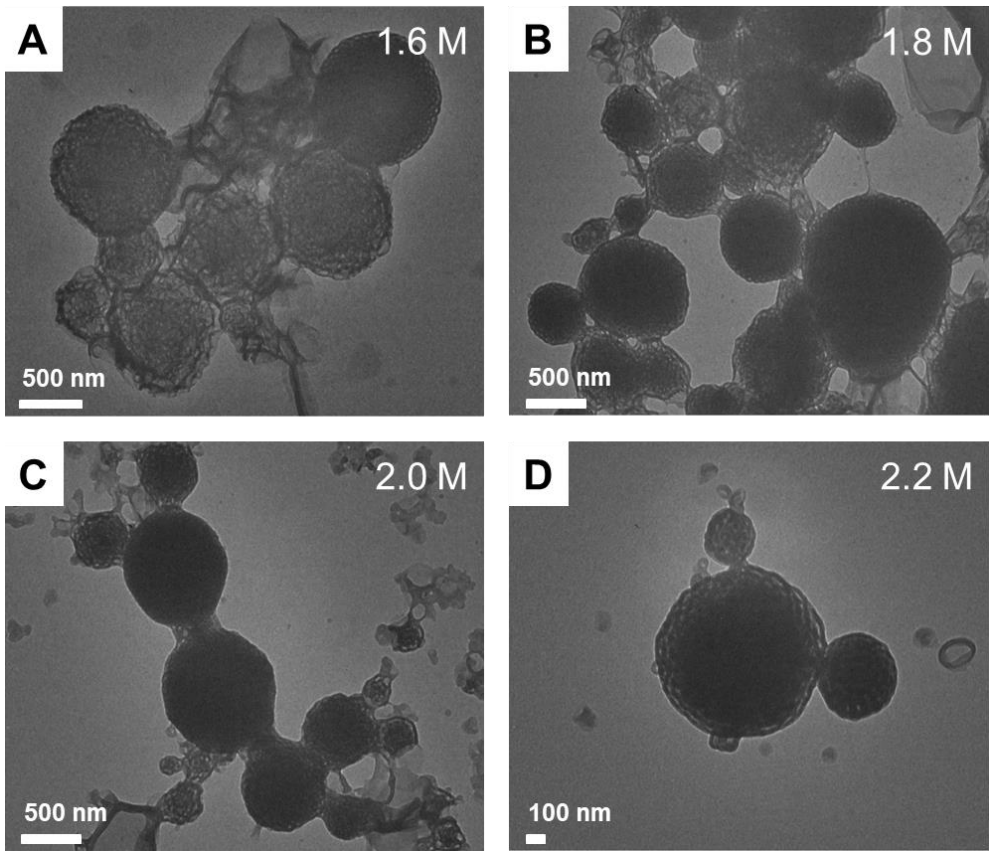

Fig. 2-26 TEM images of self-assembled structures of CE-PEG350$_3$-*b*-PS6k under different concentrations of LiCl.

2.6 REFERENCES

1 F. H. Schacher, P. A. Rupar and I. Manners, *Angew. Chem. Int. Ed.*, 2012, **51**, 7898–7921.

2 I. A. B. Pijpers, L. K. E. A. Abdelmohsen, Y. Xia, S. Cao, D. S. Williams, F. Meng, J. C. M. van Hest and Z. Zhong, *Adv. Ther.*, 2018, **1**, 1800068.

3 M. Karayianni and S. Pispas, *J. Polym. Sci.*, 2021, **59**, 1874–1891.

4 J. Gaitzsch, X. Huang and B. Voit, *Chem. Rev.*, 2016, **116**, 1053–1093.

5 D. M. Vriezema, M. C. Aragonès, J. A. A. W. Elemans, J. J. L. M. Cornelissen, A. E. Rowan and R. J. M. Nolte, *Chem. Rev.*, 2005, **105**, 1445–1490.

6 J. H. Kwon, J. Kim and K. T. Kim, *Polym. Chem.*, 2021, **12**, 2701–2711.

7 Y. La, J. Song, M. G. Jeong, A. Cho, S-M. Jin, E. Lee & K. T. Kim, *Nat. Commun.*, 2018, **9**, 5327.

8 J. Song, S. Choi, J. Lim and K. T. Kim, *RSC Adv.*, 2022, **12**, 8429–8434.

9 H. Lee, D.G. Kim, H. Ma and K. T. Kim, *Chem. Commun.*, 2020, **56**, 14059–14062.

10 J. C. M. van Hest, D. A. P. Delnoye, M. W. P. L. Baars, M. H. P. van Genderen and E. W. Meijer, *Science*, 1995, **268**, 1592–1595.

11 J. Wang, J. D. Byrne, M. E. Napier, J. M. DeSimone, *Small*, 2011, **7**, 1919–1931.

12 R. S. M. Rikken, H. Engelkamp, R. J. M. Nolte, J. C. Maan, J. C. M. van Hest, D. A. Wilson and P. C. M. Christianen, *Nat. Commun.*, 2016, **7**, 12606.

13 Y. Mai and A. Eisenberg, *Chem. Soc. Rev.*, 2012, **41**, 5969–5985.

14 C. K. Wong, X. Qiang, A. H. E. Müller and A. H. Gröschel, *Prog. Polym. Sci.*, 2020, **102**, 101211.

15 Z. Deng and S. Liu, *Polymer*, 2020, **207**, 122914.

16 S. J. Holder and N. A. J. M. Sommerdijk, *Polym. Chem.*, 2011, **2**, 1018–1028.

17 H. Chen and M-H. Li, *Macromol. Rapid Commun.*, 2021, **42**, 2100194.

18 S. Ha, Y. La and K. T. Kim, *Acc. Chem. Res.*, 2020, **53**, 620–631.

19 Z. Lin, S. Liu, W. Mao, H. Tian, N. Wang, N. Zhang, F. Tian, L. Han, X. Feng, Y. Mai, *Angew. Chem. Int. Ed.*, 2017, **56**, 7135–7140.

20 A. Blanazs, J. Madsen, G. Battaglia, A. J. Ryan and S. P. Armes, *J. Am. Chem. Soc.*, 2011, **133**, 16581–16587.

21 L. Zhang and A. Eisenberg, *Science*, 1995, **268**, 1728–1731.

22 S. J. Lee, A. Cho and K. T. Kim, *Macromol. Rapid Commun.*, 2022, 2100893.

23 O. Terreau, L. Luo and A. Eisenberg, *Langmuir*, 2003, **19**, 5601–5607.

24 P. Schuetz, M. J. Greenall, J. Bent, S. Furzeland, D. Atkins, M. F. Butler, T. C. B. McLeishd and D. M. A. Buzza, *Soft Matter*, 2011, **7**, 749–759.

25 Y. La, T. H. An, T. J. Shin, C. Park, K. T. Kim, *Angew. Chem. Int. Ed.*, 2015, **54**, 10483–10487.

26 H. Yu, X. Qiu, S. P. Nunes and K-V. Peinemann, *Nat. Commun.*, 2014, **4110**.

27 Y. Yu and A. Eisenberg, *J. Am. Chem. Soc.*, 1997, **119**, 8383–8384.

28 I. A. B. Pijpers, F. Meng, J. C. M. van Hest and L. K. E. A. Abdelmohsen, *Polym. Chem.*, 2020, **11**, 275–280.

29 X. Lyu, Z. Tang, A. Xiao, W. Zhang, H. Pan, Z. Shen and X-H. Fan, *Polym. Chem.*, 2019, **10**, 6031–6036.

30 R. Deng, M. J. Derry, C. J. Mable, Y. Ning and S. P. Armes, *J. Am. Chem. Soc.*, 2017, **139**, 7616–7623.

31 L. Zhang and A. Eisenberg, *Polym. Adv. Technol.*, 1998, **9**, 677–699.

32 L. Zhang, C. Bartels, Y. Yu, H. Shen and A. Eisenberg, *Phys. Rev. Lett.,* 1997, **79**, 5034–5037.

33 K. Yu, C. Bartels and A. Eisenberg, *Langmuir*, 1999, **15**, 7157–7167.

34 K. Yu and A. Eisenberg, *Macromolecules*, 1998, **31**, 3509–3518.

35 L. Zhang and A. Eisenberg, *Macromolecules*, 1996, **29**, 8805–8815.

36 L. Zhang, K. Yu and A. Eisenberg, *Science*, 1996, **272**, 1777–1779.

37 I. Oral and V. Abetz, *Soft Matter*, 2022, **18**, 934–937.

38 I. Oral and V. Abetz, *Macromol. Rapid Commun.,* **2021**, 42, 2000746.

39 A. Bey, O. Dreyer and V. Abetz, *Phys. Chem. Chem. Phys.*, 2017, **19**, 15924–15932.

40 D. Huang, Q. Zhang, Y. Deng, Z. Luo, B. Li, X. Shen, Z. Qi, S. Dong, Y. Ge and W. Chen, *Polym. Chem.*, 2018, **9**, 2574–2579.

41 T. Pan, J. Li, B. Li, Q. Xu, Z. Cui, J. Shang, Y. Ge and Z. Qi, *J. Phys. Chem. Lett.*, 2021, **12**, 7418–7422.

42 Z. Geng, N. S. Schauser, J. Lee, R. P. Schmeller, S. M. Barbon, R. A. Segalman, N. A. Lynd and C. J. Hawker, *Macromolecules*, 2020, **53**, 4960–4967.

43 G. Yu, K. Jie and F. Huang, *Chem. Rev.*, 2015, **115**, 7240–7303.

44 Y. Luo, N. Marets and T. Kato, *Chem. Sci.*, 2018, **9**, 608–616.

45 L. Zhang, R. J. Barlow and A. Eisenberg, *Macromolecules*, 1995, **28**, 6055–6066.

46 L. Zhang and A. Eisenberg, *J. Am. Chem. Soc.*, 1996, **118**, 3168–3181.

47 A. M. Wawro, T. Muraoka and K. Kinbara, *Polym. Chem.*, 2016, **7**, 2389−2394.

48 A. M. Wawro, T. Muraoka, M. Kato and K. Kinbara, *Org. Chem. Front.*, 2016, **3**, 1524−1534.

49 S. Ha and K. T. Kim, *Polym. Chem.*, 2019, **10**, 5805−5813.

50 S. Ha, and K. T. Kim, *RSC Adv.*, 2022, **12**, 7446−7452.

51 K. Matyjaszewski, Y. Nakagawa and S. G. Gaynor, *Macromol. Rapid Commun.*, 1997, **18**, 1057−1066.

국문초록

블록 공중합체의 자기조립 구조체 형성을 위한 막특성 조절 가능한 합성 디자인과 응용 연구

블록 공중합체의 용액 자기조립에 의해 형성된 자기조립 나노구조의 형태 조정은 약물 전달, 나노 반응기 및 나노템플릿을 포함한 잠재적 응용될 수 있었다. 또한, 분자량 분포가 없는 블록의 활용에 의해 가능한 자극 반응성 및 초분자 부분을 통합하여 합성 디자인을 통해 원하는 모양과 형태를 얻기 위해 비접촉적이고 덜 집약적인 합성 작업을 제공했다.

본 연구에서는 친수성 폴리에틸렌글리콜과 분자량 분포가 없는 소수성 올리고페닐락틱산으로 구성된 블록 공중합체는 특정한 위치에 히드라존 포토스위치를 (1) 소수성 올리고페닐락틱산 사슬의 가운데와 (2) 친수성 블록과 소수성 블록의 접합부를 합성하였다. 포토스위치는 *E-Z* 이성질화 반응을 통해 소수성 올리고페닐락틱산 블록의 입체구조 변화를

보여주었다. 특히, 고분자 막소포는 배열 활성으로 인해 자외선(UV) 또는 가시선으로 조사 시 가역적인 형상변형을 나타났다.

제 2 장에서는 트라이암 선형, 선형 및 왕관형 에터 말기 기능성 친수성 폴리에틸렌글리콜 블록과 소수성 폴리스티렌 블록으로 구성된 블록 공중합체의 합성을 보고하였다. 리튬 이온의 첨가는 구조 및 말단 그룹의 기능화된 친수성 부분을 가진 블록 공중합체에 따라 염석효과를 유발하는 진척도가 다르게 나타나는 것을 관찰하였다. 왕관형 에터와 리튬 양이온 사이의 염석효과 및 호스트-게스트 복합체의 상호작용에 의해 고분자 막소포에서 폴리머 큐보좀으로 형태변형에 상당히 기여한다는 것으로 확인하였다.

주요어 : 히드라존 포토스위치, 올리고페닐락틱산, 완관형 에터, 폴리에틸렌글리콜, 블록 공중합체, 수용액 상 자기조립, 고분자 막소포, 폴리머 큐보좀

학 번 : 2020-27163